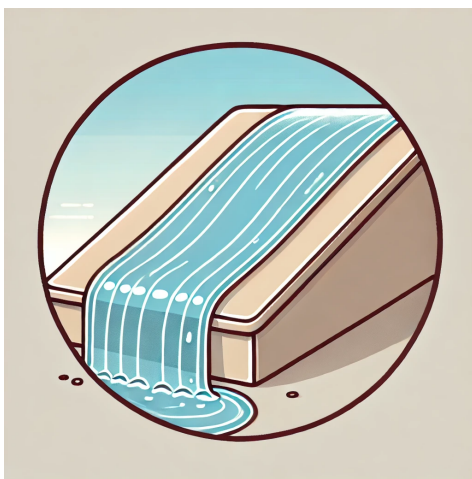# Research Visit Report

Thin Liquid Films Modelling, Simulation and Control

Bilal Ben Moussa

With the Supervision of
Dr. Susana Gomes & Dr. Radu Cimpeanu

Warwick Mathematics Institute
University of Warwick
United Kingdom
14th February 2025

Abstract

The purpose of this report is to detail what we worked on during my visit at the University of Warwick with Dr. Susana Gomes and Dr. Radu Cimpeanu in the Mathematical Institute of Warwick. First of all, we re-derived and simulated numerically a reduced-order model of the Navier-Stokes equations called the Kuramoto-Sivashinski equation. Observing its numerical behaviour allowed me to familiarize myself with a simple reduced-order model for thin film flows. Then, we focussed on the problem of stabilizing a falling liquid film with blowing air jets control, which is the main study of this report. To do so, we adapted another reduced-order model, called the Benney equation, to air jet perturbations. Then, we constructed a control from the Benney equation of the system that stabilizes the system as wanted.

Keywords: Feedback control, Stabilization, Thin liquid films, Air jets control, Asymptotic analysis, Reduced-order modelling, LQR control, Positive control.

Contents

3

1 Introduction

Thin film fluid flows are flows in which thicknesses are small compared to their length, this approximation being known as the thin film approximation. In this report, we study the stabilization of a thin fluid falling down an inclined plane of slope angle θ. Our goal is to make a wavy thin film fluid flat by the use of controlled perturbation induced by air jets. Thin film systems can typically be found in coating processes (e.g for LCD screens), heat transfer, and many more applications. These processes are used in industry, so the way of inducing perturbation must be pratical, relatively easy to set up. That is why we are using air jets as a control mechanism, as it it more covenient to use compared to blowing and suction of liquid, another way of control that we describe in the paragraph below.

The literature covering thin film systems is significantly large. Indeed, these systems provide a way to bypass the complexity of the Navier-Stokes equations by simplifying them with asymptotic theory, using the thin film approximation. Consequently, one can perform deeper mathematical studies and less computationally heavy numerical experiments, with the cost of neglecting some of the physical phenomenom described by the Navier-Stokes equation. Three types of reduced-order models, here listed with increasing complexity, are often studied: the KS (Kuramoto-Sivashinski) equation, the Benney equation, and the Weighted Residuals. These models are for example presented in the book of S.Kalliadasis and al. [9], where the authors the Benney and Weighted Residuals models in part 1.3 ("Mathematical Modeling and Methodologies"), uses the Benney methodology in chapter 5, and weighted Residual methodology in chapter 6 (see part 6.5). Naturally, simpler equations allow deeper mathematical and numerical studies of the equations. As for the control of these flows, there is a rich literature on fluid blowing and suction-based control, i.e injecting or sucking fluid from the base of the plane. In [6], Susana Gomes and al. built a control that could stabilize the KS system with a finite number of actuators to any arbitrary state including travelling waves. However, the controls derived from these equations aren't efficient for the Benney and Weighted Residual systems as the structure of the equation is probably too different. In [16], A. Thompson et al. studied proportional control and LQR control for the Benney and Weighted Residual Systems. They studied both the continuous case and discrete case, i.e with a continuum or finite number of actuators. They carried out stability analysis on the Benney and Weighted Residual systems and found that they could stabilize both systems with finite numbers of actuators and observations. Finally, O. Holroyd et al. used in [7] LQR control on Benney and Weighted Residual systems with full observations coupled with Direct Numerical Simulation (DNS) update to link the reduced-order models to more realistic simulations, which they call "numerical experiments". They found that the control works successfully beyond the linear theory stability range. Further in [8], they tackled the problem of partial observability, and likewise, built a control scheme that would stabilize the system, although in a smaller domain of Reynolds numbers. All in all, the blowing and suction method of actuation

4

is thus backed with solid results. Further improvement on this control method would probably be to test it on a 3D system, removing the periodicity along the plane axis, and test it in a real experimental setting. These improvements are obviously not easy to do and would need much work like in [3] where F. Denner et al. constructed an experimental setup and made comparisons between experimental results, DNS results and reduced-order model results.

However, blowing and sucking fluid from the base of the plane does not seem practical in an industrial context. One would need to drill several holes into the plane and create efficient fluid blowing and sucking pipes. Hence, we are interested in another way of introducing perturbation to the system: blowing air through pipes above the plane. This method seems to be more practical in an industrial framework as blowing air jet seems to be far more used and easy to construct and use than liquid blowing and sucking pipes. It introduces two main difficulties. Firstly, the control has to be positive as we want blowing air jets only. Secondly, we would need to solve the Navier-Stokes equations in the gas domain to have the link between the input power of the air jet and its effect on the liquid-gas interface which is namely the normal and tangential pressure it induces on the liquid. In [13], J. Chinasaka et al. showed with deep numerical analysis that the tangential part of the pressure has a non-negligible effect (same amplitude as 10% of the normal stress) on the liquid-gas interface of a flat water film trapped in a beacon. However, this is probably due to the fact that the water is immobile and trapped, with the air jet being strong enough to induce large deformation, until dewetting, which is not the case in our system. In [11], D. Lunz et al. studied the effects of oscillating actuators on a falling liquid film and carried out an analysis about the effect of the oscillation frequency on the gas-liquid interface. They simplified the problem by only modelling the normal stress induced by the gas on the liquid. In this report, we also chose to simplify the system and only consider normal pressure, and we justify this choice later. To the best of the author's knowledge, no control paper has been drawn up with this specific system and way of control.

The report is structured in two main parts. First, we model and observe the KS equation in part 2 as an introductory work. We solve the equation numerically using an implicit-explicit method provided in [2] and observe the main behaviours (steady states, progressive waves) of the KS equation, except its chaotic behaviour. Secondly, we study the inclined plane system: in part 3, we derive the Benney equation with a normal gas pressure control term. We introduce the normal and tangential terms of the gas stress, neglect the tangential term, and choose a classic scaling to make the normal term appear in the equation. Then, in part 4, we construct a numerical simulation scheme and carry out tests to ensure its accuracy. Finally, in part 5, we use the linearised Benney equation to compute a linear controls. We find that the LQR state feedback controls works well and stabilizes exponentially quickly the system. As the respective method gives control of any sign, we need to restrict the control to positive values to have blowing only air jets. We find that LQR optimal control with just the

positive part of the control applied at each time step stabilizes successfully the system too, although with less efficiency. However, using this method, we are not sure that the state (i.e the height the the liquid film) of the system will stay positive. Hence, we lean on another way of linear feedback control, using the theory of positive control systems.

1.1 Notations

Throughout the present document, I denote:

- dimensional quantities with a * (e.g x^*),

- non-dimensional one without anything (e.g x),

- differentiation with a ”,” e.g. $f_{,xy} = \frac{\partial^2 f}{\partial x \partial y}$.

- $\mathcal{M}_{n,m}$ (resp. $\mathcal{M}_n$) the set of real matrices with n lines and m rows (resp. n lines and n rows).

- We use all the common notations that we do not recall here (e.g the set of real numbers $\mathbb{R}$..).

- $\mathbb{R}_n[X]$ the polynomials of degree n with real coefficients and one variable X.

2 Study of the KS equation

In this section of the report, we study the Kuramoto Sivashinski (KS) equation which is known to be one of the simplest equations having chaotic behaviour. The goal of this part is not to get new results or make deep analysis as it is more an introductory part of this report. Here, we will use specific numerical scheme and change parameters to observe the various behaviours of the numerical solutions of this equation.

2.1 The system and the KS equation

The KS or Kuramoto-Sivashinski equation was first introduced by G.Sivashinski and D.M.Michelson in 1977 in [12] to describe flame fronts, and in 1978 by Y.Kuramoto in [10] to study chaotic behaviors in chemical reactions. Several other type of KS equation exists, e.g stochastic KS equation that adds a linear stochastic term. For more details, see the thesis of Dr.Susana Gomes [5] to see the study of several type of KS equations.

One of its versions is

$$\begin{cases} u_{,t} + u_{,xxxx} + u_{,xx} + uu_{,x} = 0, \\ \qquad\qquad u(x + L) = u(x). \end{cases} \tag{1}$$

Here, we use this equation to model falling liquid flowing down an inclined plane in a 2D setting. The plane has a finite length L along its axis, the x-axis, which constitutes the flowing direction of the liquid. We consider the liquid being L-periodic. The KS equation can be derived from the Benney equation, which is a reduced-order equation obtained from the 2D Navier Stokes equations. The Benney equation is presented later in part 3. We put the derivation of the KS equation in appendix.

Here, nor the slope angle θ or other parameters like Reynolds or Capillary numbers appear due to the way the KS equation is derived as the change of variable (not possible for all value of Reynolds number and theta) make all the variables disappear and the only variable which can be changed is the nondimensionnal length L of the domain.

Description of the terms. One of the benefits of the KS equation is that it is a weakly non linear equation which means that its non-linearities, here $uu_{,x}$ aren't too complex compared to other long wave models like the Benney or the Weighted Residuals one. In one hand, the simple character of the non lineariy in the KS equation allows deep mathematical studies, as said before in the introduction (part 1). Nevertheless, the non linear aspect seems to bring complex behaviours, here chaotic one. This non linearity is called "Burger non linearity" referring to the Burgers equation:

$$\begin{cases} y_{,t}(x, t) + yy_{,x}(x, t) = 0, \quad (x, t) \in \mathbb{R} \times \mathbb{R}_+ \\ \qquad\qquad\qquad y(., t = 0) = y_0(.) \end{cases}$$

where the non-linear term is the same as in the KS equation.

Rescaling. Let introduce what we call the instability parameter

$$\nu = \left(\frac{2\pi}{L}\right)^2. \tag{2}$$

We make the change of variable:

$$\tilde{x} = \frac{2\pi}{L}x = \frac{x}{\sqrt{\nu}}, \quad \tilde{t} = \left(\frac{2\pi}{L}\right)^2 t = \frac{t}{\nu}, \quad \tilde{u} = \frac{L}{2\pi}u = \sqrt{\nu}u. \tag{3}$$

We keep the same notation and remove the " ˜ " from the letters. We are now studying an equation on the domain $[0, 2\pi)$ and not $[0,L)$:

$$\begin{cases} u_{,t} + \nu u_{,xxxx} + u_{,xx} + uu_{,x} = 0 \\ \qquad\qquad u(x + 2\pi) = u(x). \end{cases} \tag{4}$$

We see that the factor ν appeared in the equation. Its value will change the behaviour of the numerical solution, from steady states to chaos, as we will see in the simulations. That is why it is called "instability parameter".

The system. We are studying this equation in the domain $[0, 2\pi)$ which is equivalent to study it on $[0, L)$ with $L = \frac{2\pi}{\sqrt{\nu}}$. We will input periodic sinusoidal initial conditions and observe how they will behave depending on the frequency of the initial condition and the value of ν. We do not set a particular final time T as it could change depending on what we want to see.

2.2 The numerical scheme

In this section, we use the scheme described in [2]. In the cited paper, the authors use it for a more complex system of equations as they try to model the dynamics of the fluids height and a surfactant. Here, we do not justify that the numerical scheme is appropriate for the KS equation, at the opposite of [2] . To do so, one would need to prove the regularity of the linear and non linear operators in the KS equation, which would be a specific case of [2] with a null surfactant concentration.

2.2.1 Decomposition in Fourier series

We rewrite the KS equation (4):

$$\begin{cases} u_{,t} + \nu u_{,xxxx} + u_{,xx} + \dfrac{1}{\nu}u = \dfrac{1}{\nu}u - uu_{,x}, \\ \qquad\qquad u(x + 2\pi) = u(x). \end{cases} \tag{5}$$

We added the $\frac{1}{\nu}u$ term because we reproduced the scheme constructed in [2]. It is used in the implicit-explicit numerical scheme of [1] where the left part will be implicit

8

and the right one explicit.

As the function u in the KS equation (4) is 2π-periodic, we decompose it into its Fourier series. As u is real, we can decompose it for sin and cos components:

$$u(x,t) = \sum_{j=1}^{+\infty} u_j^c \cos(jx) + u_j^s \sin(jx) + \bar{u}(t), \tag{6}$$

$$u^c = (u_j^c)_{j \in \mathbb{N}^*}, u^s = (u_j^s)_{j \in \mathbb{N}^*}, \bar{u},$$

being respectively the cos, sin components and the mean value of u.

As we study the steady state u=0, we take centered sinusoidal initial conditions, so we have that

$$\bar{u} = 0.$$

Using the Fourier series in (4), we get

$$u_{,t} + \nu u_{,xxxx} + u_{,xx} + \frac{1}{\nu}u = \sum_{j=1}^{\infty} \left(\frac{du_j^c}{dt} + (\nu j^4 - j^2)u_j^c + \frac{1}{\nu}u_j^c\right)\cos(jx)$$

$$+ \sum_{j=1}^{\infty} \left(\frac{du_j^s}{dt} + (\nu j^4 - j^2)u_j^s + \frac{1}{\nu}u_j^s\right)\sin(jx)$$

$$= \sum_{j=1}^{\infty} \left(\frac{1}{\nu}u_j^c - F_j^c\right)\cos(jx) + \left(\frac{1}{\nu}u_j^s - F_j^s\right)\sin(jx)$$

$$= \frac{1}{\nu}u - uu_{,x},$$

with

$$F_j^c = -\frac{j}{2} \sum_{m+n=j} u_m^c u_n^s + \frac{j}{2} \sum_{m-n=j} (u_m^c u_n^s - u_n^c u_m^s),$$

$$F_j^s = \frac{j}{4} \sum_{m+n=j} (u_m^c u_n^c - u_m^s u_n^s) + \frac{j}{2} \sum_{m-n=j} (u_m^c u_n^c + u_n^s u_m^s),$$

the Fourier cross terms induced by the weak non-linearity of the KS equation.

By projecting the inequality on $\left((\cos(jx))_{j \in \mathbb{N}^*}, (\sin(jx))_{j \in \mathbb{N}^*}\right)$, orthogonal family of vectors in $L^2([0, 2\pi), \mathbb{R})$, we have an infinite number of ordinal differential equations (ODEs):

$$\forall j \in \mathbb{N}^*, \quad \begin{cases} \dfrac{du_j^c}{dt} + (\lambda_j + \dfrac{1}{\nu})u_j^c = \dfrac{1}{\nu}u_j^c + F_j^c, \\ \dfrac{du_j^s}{dt} + (\lambda_j + \dfrac{1}{\nu})u_j^s = \dfrac{1}{\nu}u_j^c + F_j^s, \end{cases} \tag{7}$$

9

with

$$\forall j \in \mathbb{N}^*, \quad \lambda_j = \nu j^4 - j^2 = \nu j^2 (j - \frac{1}{\sqrt{\nu}})(j + \frac{1}{\sqrt{\nu}}). \tag{8}$$

We do not simplify the u_j^c, u_j^s in the equation as one will be implicit and the other explicit in the numerical scheme that we will describe in an instant.

Let us underline that the equations in (7) have exponential solutions of rate λ_j when there is no weak non linearity terms $F_j^{c,s}$ i.e equations of the form

$$\forall j \in \mathbb{N}, \quad \frac{du_j^{c,s}}{dt} = -\lambda_j u_j^{c,s}. \tag{9}$$

Sign of $\boldsymbol{\lambda_j}$. If we neglect the non-linearities, we notice that we would have an exponential dampening on the jth mode if and only if

$$-\lambda_j < 0.$$

When $\forall j \in \mathbb{N}^*, -\lambda_j < 0$, we are expecting the non-linearities to be indeed negligible if we take a low number of initial mode as the the $F_j^{c,s}$ will be small at the beginning so the derivatives of the $u_j^{c,s}$ will still be negative. At the opposite, if there exists j in $\mathbb{N}$ such that $-\lambda_j > 0$, then, if we take the non-linearities small enough at the beginning, u_j will grow and its effect will spread in the other u_i through the non-linearities F_j^c and F_j^s. Therefore, we will try later to test cases with different signs of the λ_j by changing the parameter ν.

2.3 Description of the scheme

Here, we first present the equations (7) in a specific way, discretize them for them to be suitable for numerical program, and then introduce the numerical scheme that we are going to use.

we set

$$U = (u^c, u^s) \in \mathbb{R}^{\mathbb{N}^*} \times \mathbb{R}^{\mathbb{N}^*} \tag{10}$$

the grouping of the 2 Fourier coefficients vectors u.

Equations (7) can be rewritten as

$$\frac{dU}{dt} + A(U) = B(U), \tag{11}$$

with

$$AU = \left((\lambda_j + \frac{1}{\nu})u_j^c, (\lambda_j + \frac{1}{\nu})u_j^c \right)_{j \in \mathbb{N}}, \quad B(U) = \left(\frac{1}{\nu}u_j^c + F_j^c, \frac{1}{\nu}u_j^s + F_j^s \right)_{j \in \mathbb{N}},$$

so A and B are respectively a linear and a non-linear operators.

The numerical Scheme. We describe now the numerical scheme used by [2]. They used a implicit-explicit multi-step method introduced and analyzed in [1] by G.Akrivis and M.Crouzeix. We will see it is an implicit BDF (Backward Differentiation Formula) scheme of order

$$p_{BDF} \in \mathbb{N}^* \tag{12}$$

for the time derivative and the linearity, combined with a multi-step explicit scheme for the non-linearity.

Let us now set N_x, N_t the number of space and time points respectively. Then the time and space steps are respectively

$$dt = \frac{T}{N_t - 1}, \quad dx = \frac{2\pi}{N_x}.$$

Let us then set

$$\forall n \in [|0, N_t - 1|], \quad U^n := U(ndt) = \Big((u_j^c(ndt))_{j\in\mathbb{N}}, (u_j^s(ndt))_{j\in\mathbb{N}}\Big).$$

We introduce the polynomials of degree p_{BDF}

$$\alpha = \sum_{i=1}^{p_{BDF}} \frac{1}{j} X^{p_{BDF}-1}(X-1)^j, \quad \beta = X^{p_{BDF}}, \quad \gamma = X_{BDF}^p - (X-1)^{p_{BDF}} \in \mathbb{R}_{p_{BDF}}[X]. \tag{13}$$

The numerical scheme for the time is constructed with the coefficients of α and β with and implicit scheme whereas the non linearity is discretized with the coefficient of α and γ explicitly (no $U^{n+p_{BDF}}$). Both schemes are of order p_{BDF}:

$$\sum_{i=0}^{p_{BDF}} \alpha_i U^{n+i} + dt\beta_{p_{BDF}} A U^{n+p_{BDF}} = dt \sum_{i=0}^{p_{BDF}-1} \gamma_i B(U^{n+i}), \quad n \in [|0, N - p_{BDF}|] \tag{14}$$

with $\alpha_i, \beta_i, \gamma_i$ being the coefficients of order i of α, β, and γ respectively. Hence the scheme is:

$$\boxed{\sum_{i=0}^{p_{BDF}} \alpha_i U^{n+i} + dt A U^{n+p_{BDF}} = dt \sum_{i=0}^{p_{BDF}-1} \gamma_i B(U^{n+i}), \quad n \in [|0, N - p_{BDF}|]} \tag{15}$$

Now we truncate U up to a certain order to carry on numerical computations. Like in [2] we denote the truncated counterpart $U^{n,M}$ with an additional M which would be the highest mode taken into account in the simulation. We get

$$U^{n,M} = \Big((u_j^c(ndt))_{j\in[|1,d|]}, (u_j^s(ndt))_{j\in[|1,M|]}\Big) \in \mathbb{R}^{2M},$$

A^M and B^M the new operators defined naturally from A and B with the new truncated non linear coefficients:

$$\begin{cases} F_j^{c,M} = -\dfrac{j}{2} \displaystyle\sum_{\substack{m+n=j \\ 0 \leq m,n \leq M}} u_m^c u_n^s + \dfrac{j}{2} \displaystyle\sum_{\substack{m-n=j \\ 0 \leq m,n \leq M}} (u_m^c u_n^s - u_n^c u_m^s) \\ F_j^{s,M} = \dfrac{j}{4} \displaystyle\sum_{\substack{m+n=j \\ 0 \leq m,n \leq M}} (u_m^c u_n^c - u_m^s u_n^s) + \dfrac{j}{2} \displaystyle\sum_{\substack{m-n=j \\ 0 \leq m,n \leq M}} (u_m^c u_n^c + u_n^s u_m^s) \end{cases} . \quad (16)$$

As we use the FFT algorithm (Fast Fourier Transform), the highest mode left is $M = \lfloor N_x/2 \rfloor$.

2.4 Simulations and Results

We implemented all the simulations in a python file. For more precision on the code, see the appendix A.1 on how we implemented it, or see also the code in itself on the Github page.

2.4.1 Dispersion relation

We recall the expression of the $-\lambda_j$:

$$-\lambda_j = -\nu j^2 (j - \frac{1}{\sqrt{\nu}})(j + \frac{1}{\sqrt{\nu}}). \quad (17)$$

As it was said previously, we want to know the sign of the $-\lambda_j$ to have an idea of the behaviour of the system .By analysing the polynomials of order 4 in j, we have that

$$\begin{cases} -\lambda(j) > 0 \quad \text{on } (0, \dfrac{1}{\nu}) \quad \text{(exp. growth)}, \\ -\lambda(j) < 0 \quad \text{on } (\dfrac{1}{\nu}, +\infty) \quad \text{(exp. decay)}, \\ \qquad\qquad -\lambda(j) = 0 \quad \text{on } \{0, \dfrac{1}{\sqrt{\nu}}\}. \end{cases} \quad (18)$$

Let us note that for $\nu \geq 1$, having j in $\mathbb{N}^*$ such that $-\lambda_j > 0$ is impossible. As we study a periodic function, it is a superposition of natural integer modes (cf the Fourier series of u in (6)) so we are not interested in non natural number modes i.e $j \notin \mathbb{N}$. Hence, any periodical input would be exponentially dampened in a system with $\nu < 1$ if there were no non linearities.

We show on figure 1 two profiles of λ_j for different values of ν, with and without divergent modes. We will now separate our observations in two parts: $\nu \geq 1$ and $\nu < 1$.
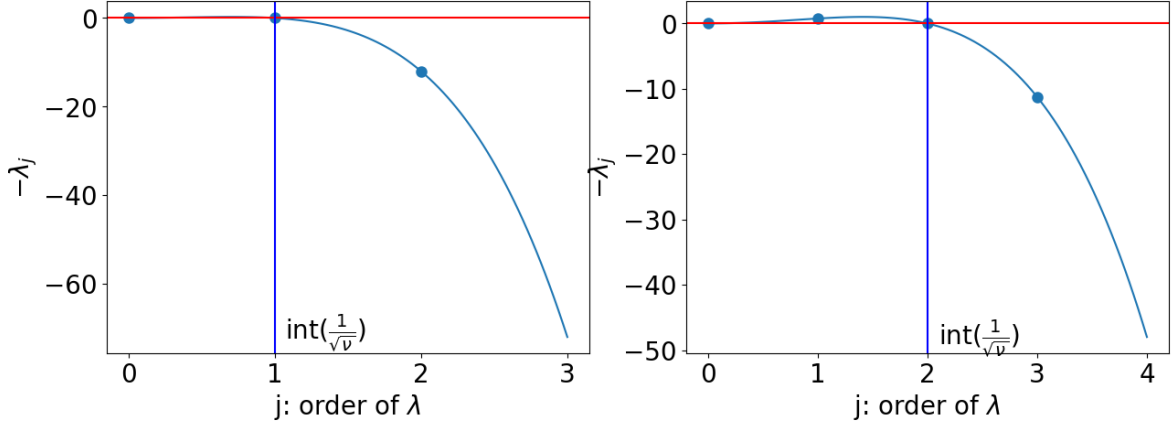
12

Figure 1: Two curves of $-\lambda_j = -\nu j^2(j - \frac{1}{\sqrt{\nu}})(j + \frac{1}{\sqrt{\nu}})$ for $\nu = 1$ and $\nu = \frac{1}{4}$. As expected, we have all the $-\lambda_j$ non positive for $j \in \mathbb{N}$ for the case $\nu \leq 1$ that could maybe give an exponential decreasing. As for the case $\nu < 1$, we see that $-\lambda_1 > 0$ so the first mode can possibly grow at the begining if the non linear terms are not to large and negative.

2.4.2 $\nu \geq 1$

As said before, we are expecting the system to have a behaviour similar to an exponential decay. Here, we measure the characteristic decay of curves as if they were decaying exponentially by computing an exponential regression i.e a linear regression on the logarithm of the quantity. Then, we compare the coefficients to the expected rate.

We carry out these tests for $\nu = 1$. We compared the dampening values for $k \in \{0, 1, 2, 3, 4, 5\}$. We set an the initial condition sin(kx) and cos(kx). Except for k=0, we found that for both initial conditions, the exponential regime and the curve of u_{max} were identical until a floor value (around 10^{-16}) where the solution would become flat. We think that one calculus in the numerical scheme may have led to a numerical zero which nullified the time derivative, which would explain why the numerical solution reaches a flat state.

If we had an exponential regime,

$$\log(u_{max}) \approx \log(u_{max}(0)e^{-\lambda_k t}) = \log(u_{max}(0)) - \lambda_k t,$$

with $u_{max}(t) = \max_{x \in [0,2\pi]} |u(.,t)|$. Hence, we make the linear regression of $log(u_{max}) \approx at + b$ and we compare the coefficient a and b to $-\lambda_k$ and $log(u_{max}(0))$ respectively with these relative errors terms:

$$\eta_a = \frac{|a - (-\lambda_k)|}{|-\lambda_k|}, \eta_b = \frac{|b - \log(u_{max}(0))|}{|\log(u_{max}(0))|}.$$

The determination coefficient r^2 of the linear regression was always very high (at least

13

Modes j	η_a (in %)	η_b (in %)
2	$(0.04, 0.2)$	$(0.4, 2)$
3	$(2.10^{-4}, 2.10^{-3})$	$(0.01, 0.05)$
4	$(1.10^{-6}, 1.10^{-5})$	$(0.01, 0.01)$

Table 1: Table of the error terms $\eta_a = \frac{|a-(-\lambda_k)|}{|-\lambda_k|}, \eta_b = \frac{|b-\log(u_{max}(0))|}{|\log(u_{max}(0))|}$ for $(\cos(kx), \sin(kx))$ as initial condition, for $k \in \{2, 3, 4\}$.

0.9999 [1]$)$ so we do not display it.

We see that the errors terms η_a, η_b are very low so the non-linearities in that case are quite negligible. We see that the errors are a bit higher if we take sin as initial condition compared to cos. This is probably because they are no crossed term (i.e $u_m^s u_n^c$ and not $u_m^c u_n^c$) in the non linearity F_j^s than in F_j^s. For instance, if we take $\sin(2x)$ as initial condition, non zero terms will appear in $F_4^s = \frac{4}{4}(-u_2^{s2})$ but $F_4^c = 0$. This is the case for an infinite number of modes after j=2. Therefore, the effect of the non-linearities appears the most for little modes as they make higher modes appear which creates a chain reaction . That is maybe why the relative error rate are decreasing when we test higher modes.
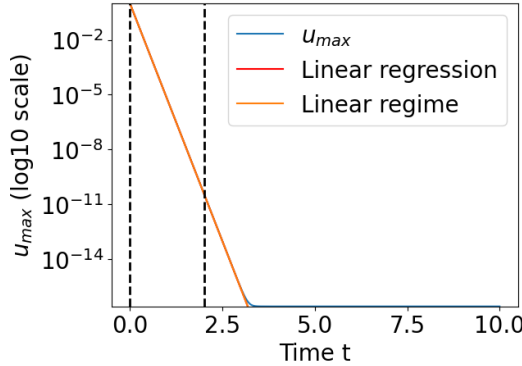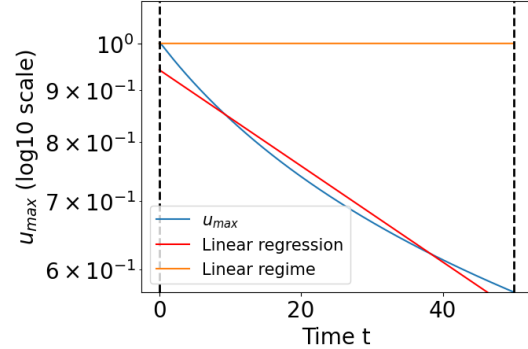

Figure 2: Case nu=1, k=2

Figure 3: Case nu=1, k=1

Figure 4: Plot of the exponential decay of $\max |u(., t)|$ in $\log_{10}$ scale and its comparison with the exponential regime obtain by removing the non- linearities. The initial condition is, in the right graph, a mode of order $k = 1$ i.e cos or sin and, on the left graph, a mode of order $k = 2$. The left part behave exactly like the exponential regime. As for the right plot, the expected exponential regime is a steady state with $u_{max} = 1$ which can be seen at the top of the graph. However, we observe that the initial condition decreases in norm because of the non-linearities. The black horizontal dots are delimiting the domain where the linear regression has been made.

In opposite to the previous cases, the case $j = 1$ is different to the linear regime

---

[1]$r^2 = 1$ being a perfect matching

which should be just stationary. In the same spirit than the remark above, we think that all the non-linearities $F_{j'}$ of the modes after $j' > j = 1$ are non zero. The main mode $j = 1$ do not become small quickly like the previous cases, so the non-linearities $F_{j'}$ become non negligible too and make the function non stationary. However, we do not know why they make the function decrease as it is not obvious that the non linearities should be negative in this case.

2.4.3 $\nu < 1$

We now look at the case $\nu < 1$. It is expected to have far more complex behaviour than when $\nu \geq 1$ as we can have here exponentially growing modes interacting with each other. We observe that the system seems to be more unstable with $\nu = (\frac{2\pi}{L})^2$ decreasing, i.e when L increases. We notice three behaviours: exponential dampening (linear regime), stabilization around a non-zero steady state, and a progressive wave.

In opposition to the tests above, we are fixing a mode value (e.g $j = 1$) and change the value of ν. We show in figure 5 a plot of $\nu \mapsto -\lambda_k(\nu)$ with $k \in \{1, 2, 3, 4\}$ and $\nu < 1$.
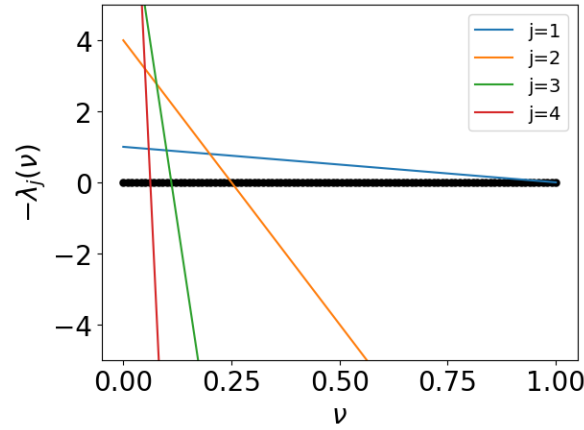
Figure 5: Plot of $-\lambda_j(\nu) = -\nu j^2(j^2 - 1)$, $j \in \{1, 2, 3, 4\}$ as a function of ν.
We see that there are more and more positive modes when ν decreases. Furthermore, the equation is more sensitive when ν is small compared to ν near 1 as the same perturbation $\delta\nu$ around small ν could give several additional pseudo exponential growing modes.

We see in (5) that the case $\nu = \frac{1}{4}$ gives a second divergent mode $k = 2$. We carry out tests with ν getting closer to 1/4 by above ($\{\frac{1}{2}, \frac{1}{3}, \frac{7}{24} = \frac{1/3 + 1/4}{2}, \frac{13}{48} = \frac{7/24 + 1/4}{2}\}$). We observe two behaviours:

- When ν is "far" from $\frac{1}{4}$: u grows exponentially and then stabilizes around a wavy steady state.

15

Figure 6: Plot of $\max(|u_s(.,t)|), \max(|u_c(.,t)|)$ with $k = 1$ (cos as initial condition, which can be seen at time $t = 0$), $\nu = \frac{13}{48}$.
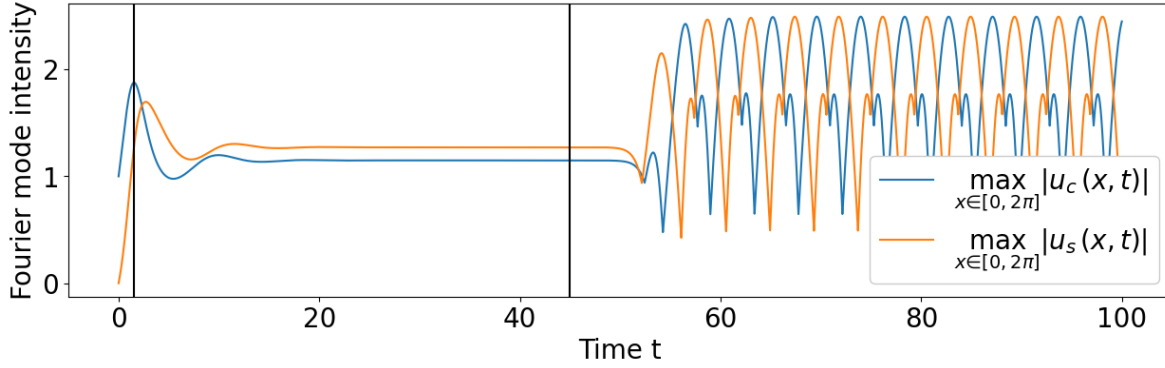
We can see here 3 behaviours. First, the numerical solution u grows, then, decreases and stabilizes around a non-zero steady state to finally turn into a travelling wave. Indeed, we can see that the extrema of the cos and sin parts of the Fourier modes are oscillating at a fixed frequency. This travelling wave can be seen in a video on the Github repository.

- When ν is "close" to $\frac{1}{4}$: In the same way, there is an exponential growing and a stabilization around a non-zero steady state. However the equilibrium breaks and it becomes a traveling wave as we can see in figure 6.

We do not go further for this little study of the KS equation. We analyzed this weakly linear equation through the Fourier decomposition of u and tried to interpret the numerical results by observing the equation through each mode as being similar to an exponential regime. The case $\nu \geq 1$ seemed to give simple result of exponential decay, while the case $\nu < 1$ was more difficult to interpret as modes are influencing each other in a non negligible way. The numerical solution had indeed a more complex behaviour as it would stabilize around non-sero steady state or turn into a traveling wave.

We didn't test the case $\nu < \frac{1}{4}$. The KS equation seems to be more unstable as ν decreases, i.e when L increase. Hence, the domain $\nu \in (0, \frac{1}{4}]$ should be even richer in term of behaviour as we add other exponentially growing modes.

As the KS equation is weakly linear, many mathematical studies have been carried out to study its chaotic behaviour (that we do not see here), like the study of bifurcation. We again refer to the thesis of Dr.Gomes [5] for a real study of this equation and its various versions.

3 The Benney equation with air jets actuators

3.1 Derivation of the Benney Equations without control

We are studying a liquid flowing down an inclined plane of angle θ from the horizontal. We limit ourselves to the 2D problem by studying the 1D liquid film flowing down the plane (now a line). The system of axis (x^*, y^*) is direct, with x^* pointing downstream and y^* being normal to the plane.

Governing equations. We study

The Navier-Stokes equations (Second law of Newton and incompressibility equation):

$$\begin{cases} \rho(u^*_{,t^*} + u^* u^*_{,x^*} + v^* u^*_{,y^*}) = -p^*_{,x^*} + \mu_l(u^*_{,x^*x^*} + u^*_{,y^*y^*}) + \rho sin(\theta)g \\ \rho(v^*_{,t^*} + u^* v^*_{,x^*} + v^* v^*_{,y^*}) = -p^*_{,y^*} + \mu_l(v^*_{,x^*x^*} + v^*_{,y^*y^*}) - \rho cos(\theta)g \\ u^*_{,x^*} + v^*_{,y^*} = 0 \end{cases} \qquad (19)$$

We take a no slip boundary conditions at the wall so at y $= 0$[2]:

$$u^* = 0, v^* = 0. \qquad (20)$$

The normal and tangential Dynamic Boundary Condition or the dynamic stress balance at the interface are :

$$\begin{cases} -p^*_l + \dfrac{2\mu_l}{1 + h^{*}_{,x^*}{}^2}(u^*_{,x^*}h^{*}_{,x^*}{}^2 - h^*_{,x^*}(u^*_{,y^*} + v^*_{,x^*}) + v^*_{,y^*}) = \dfrac{\gamma h^*_{,x^*x^*}}{(1 + h^{*}_{,x^*}{}^2)^{3/2}}, \\ (v^*_{,x^*} + u^*_{,y^*})(1 - h^{*}_{,x^*}{}^2) + 2h^*_{,x^*}(v^*_{,y^*} - u^*_{,x^*}) = 0. \end{cases} \qquad (21)$$

The Kinematic Boundary condition:

$$h^*_{,t^*} = v^* - u^* h^*_{,x^*}. \qquad (22)$$

Nondimensionalisation and scaling.
We now make a change of variable in order to manipulate dimensionless quantities. We denote

- $\mathcal{L}^*$ characteristic horizontal length

- $\mathcal{H}^* = h^*_N$ typical fluid height (and typical vertical length) which is also the *Nusselt solution* which is the height of the uniform steady solution of the equations

---

[2]in the case of a control with blowing and suction from the plane, $v^* \neq 0$

- $\mathcal{U}^* := U_N^* = \frac{\rho g h_N^{*\,2} \sin(\theta)}{2\mu_l}$ velocity of the Nusselt solution.

- $\mathcal{P}^*$ typical pressure of the liquid

Moreover, we make the **Thin–Film Approximation** which is to take $\mathcal{H}^* \ll \mathcal{L}^*$ i.e the width of the film is small compared to its length. We now scale the variables of the problem with the **thin-film parameter**

$$\boxed{\epsilon = \frac{\mathcal{H}^*}{\mathcal{L}^*}.} \tag{23}$$

Therefore, we get this system of non-dimensional quantities::

$$
\begin{aligned}
x^* &= \mathcal{L}^* x, \quad y^* = \epsilon \mathcal{L}^* y, \\
u^* &= \mathcal{U}^* u, \quad v^* = \epsilon \mathcal{U}^* v, \\
p_l^* &= \mathcal{P}^* p_l,
\end{aligned}
$$

where we took the typical vertical velocity equal to $\mathcal{V}^* := \epsilon \mathcal{U}^*$. We now take some convenient form for the typical pressure: $\mathcal{P}^* = \frac{\mu_l U^*}{h_N^*}$ and set the nondimensionalised quantities (Reynolds and Capillary numbers):

$$\boxed{Re = \frac{\rho \mathcal{U}^* h_N}{\mu_l}, \quad Ca = \frac{\mu_l \mathcal{U}^*}{\gamma}.} \tag{24}$$

We choose the **scaling**

$$\boxed{Re = O(1) \text{ and } Ca = O(\epsilon^2).} \tag{25}$$

The first scaling allow to consider inertia whereas the second one underlines the effect of surface tension in the order 1 approximation in ϵ that is used to derive the Benney equations. Indeed, the effect of interest here are **viscosity**, **surface tension**, **gravity** and **inertia**. These 4 effects are balanced by the 3 quantities Re, Ca and U_N the Nusselt velocity which is a function of the slope angle θ.

Non-dimensional governing equations. We present now the new equation with dimensionless variables.

First, we have the Navier-Stokes equation:

$$
\begin{cases}
Re(u_{,t} + u u_{,x} + v u_{,y}) = -p_{,x} + u_{,xx} + u_{,yy} + 2, \\
Re(u_{,t} + u u_{,x} + v u_{,y}) = -p_{,x} + u_{,xx} + u_{,yy} + 2 + v_{,yy} - \rho \cos(\theta) g, \\
\quad u_{,x} + v_{,y} = 0.
\end{cases} \tag{26}
$$

18

Then, the no slip condition:

$$u = 0, \quad v = 0 \quad \text{at y=0}. \tag{27}$$

The Dynamic stress balance at the interface:

$$
\begin{cases}
-p_l + \dfrac{2}{1 + h_{,x}{}^2}(u_{,x}h_{,x}{}^2 - h_{,x}(u_{,y} + v_{,x}) + v_{,y}) = \dfrac{1}{Ca}\dfrac{h_{,xx}}{(1 + h_{,x}{}^2)^{3/2}}, \\
(v_{,x} + u_{,y})(1 - h_{,x}{}^2) + 2h_{,x}(v_{,y} - u_{,x}) = 0.
\end{cases}
\tag{28}
$$

Finally, the Kinematic Boundary condition (KBC):

$$h_{,t} = v - uh_{,x}. \tag{29}$$

From (29) and (26) and (27), i.e the KBC, incompressibility, and no slip equations, we can construct the 1D mass conservation equation:

$$h_{,t} + q_{,x} = 0, \tag{30}$$

with

$$q(x,t) = \int_{y=0}^{h_{(x,t)}} u(x,y,t)dy, \tag{31}$$

being the horizontal flux of the flowing liquid.

Benney equation.
With the chosen scaling, we perform order 1 asymptotics in ϵ on the governing equations and compute the order 1 flux. These computations can be found in the appendix of the paper of A.Thompson and al. [15]. It leads us to the so called Benney equations:

$$
\begin{cases}
h_{,t} + q_{,x} = 0, \\
q(x,t) = \dfrac{h^3}{3}\left(2 - 2h_{,x}\cot(\theta) + \dfrac{h_{,xxx}}{Ca}\right) + Re\dfrac{8h^6 h_{,x}}{15}.
\end{cases}
\tag{32}
$$

Or, explicitly with the variable h[3]:

$$
\begin{aligned}
&h_{,t} + h_{,x}h^2\left(2 - 2h_{,x}\cot(\theta) + \dfrac{h_{,xxx}}{Ca}\right) \\
&- \dfrac{h^3}{3}\left(2h_{,xx}\cot(\theta) - \dfrac{h_{,xxxx}}{Ca}\right) + \dfrac{8Re}{15}\left(6h^5 h_{,x}{}^2 + h^6 h_{,xx}\right) = 0.
\end{aligned}
\tag{33}
$$

---

[3]For another reduced-order model called Weighted Residuals, the system of equation is not explicit with respect to the height h, so the unknown are the height h and the flux q.

3.2 Benney equation with a control term

We want to stabilize the fluid by applying some air jet controlled perturbation. However, we do not model the air and just take a specific form of the normal pressure (which will be defined later with a shape function d in (74)).

Tangential and Normal component of the air jet. Let

$$\underline{s_g} = -\underline{n}.\underline{\underline{\sigma_l}} \tag{34}$$

the strain vector on the normal component of the liquid-gas interface. Here, $\underline{\underline{\sigma_l}}$ is the Cauchy strain tensor of the liquid, and $\underline{n}$ is the normal from the liquid to the gas. We take as normal and tangential vectors $(\underline{n}, \underline{t})$ a normalized, orthogonal and direct couple. We then isolate the normal and tangential components of the external gas pressure:

$$\underline{n} = \frac{1}{\sqrt{1 + h_{,x}^2}}(-h_{,x}, 1), \quad \underline{t} = \sqrt{1 + h_{,x}^2}(1, h_{,x}), \tag{35}$$

$$\boxed{(N_s, T_s) = \underline{s_g}(y = h).\underline{n}.} \tag{36}$$

Let us emphasize that we took the sign convention of N_s such that it is positive with a compressive force, as $\underline{s_g}$ is defined with a $-\underline{n}$ which points from the gas to the liquid.

As for the governing equations, only the KBC changes:

$$\begin{cases} -p_l + \dfrac{2}{1 + h_{,x}^2}(u_{,x} h_{,x}^2 - h_{,x}(u_{,y} + v_{,x}) + v_{,y}) = \dfrac{1}{Ca}\dfrac{h_{,xx}}{(1 + h_{,x}^2)^{3/2}} - N_s, \\[2mm] \dfrac{(v_{,x} + u_{,y})(1 - h_{,x}^2) + 2h_{,x}(v_{,y} - u_{,x})}{1 + h_{,x}^2} = -T_s. \end{cases} \tag{37}$$

Howewer, only the normal component of the KBC changes in reality as we take

$$\boxed{T_s = 0,} \tag{38}$$

which means that we neglect the tangential part of the stress of the gas on the liquid. This approximation has been made by the paper of D.Lunz & al. [11], but it has been shown on another system studied by Chinasa J. Ojiako & al. in ([13]) that the tangential component of the air jet pressure has non negligible effects on the profile of the liquid-gas interface. We decide not to take into account the tangential stress for two reasons.

- First, we think that the tangential part of the air stress on the liquid was non negligible (around 10% of the normal stress N_s) in the case of the paper of Chinasa J. Ojiako and al. because the air was blown on immobile flat water trapped into a

beacon, so the trough produced by the air jet would prevent air from escaping by the sides. In other words, we think that this competition between the liquid and the air trying to escape makes T_s non negligible. This effect is probably largely attenuated in our system since the fluids are here driven by gravity and inertia, so there are much fluid movement that would allow the gas to come out easily by the sides.

- Secondly, considering T_s would add too much complexity to our model. We prefer to construct a simple model on which we can apply a control strategy more easily. Another work about constructing an equation and control strategy while taking into account T_s could be made and compared to this one.

Benney equation with control. The computation of the pressure is different (cf appendix C.1) and it gives at order 1 in ϵ:

$$
\begin{cases}
h_{,t} + q_{,x} = 0, \\[2mm]
q(x,t) = \dfrac{h^3}{3}(2 - p_{l0,x}) + Re\dfrac{8h^6 h_{x,}}{15},
\end{cases}
\tag{39}
$$

with

$$
p_{l0} = N_s + 2(h - y)cot(\theta) - \frac{h_{,xx}}{Ca}
\tag{40}
$$

the pressure term approximated at order 0 in ϵ.

Hence, the Benney equation with only h as unknown is

$$
\begin{aligned}
&h_{,t} + h_{,x}h^2\left(2 - N_{s,x} - 2h_{,x}cot(\theta) + \frac{h_{,xxx}}{Ca}\right) \\[2mm]
&- \frac{h^3}{3}\left(N_{s,xx} + 2h_{,xx}cot(\theta) - \frac{h_{,xxxx}}{Ca}\right) + \frac{8Re}{15}\left(6h^5 h_{,x}{}^2 + h^6 h_{,xx}\right) = 0.
\end{aligned}
\tag{41}
$$

3.3 Linear Theory

In this section, we present some theory relying on the linearisation of the Benney equation.

We write the height as a perturbed state from the normalized Nusselt height $h_N = 1$:

$$
h = 1 + \delta\tilde{h}, \quad N_s = \delta\tilde{N}_s.
\tag{42}
$$

Let us underline that δ and ϵ aren't linked. The ϵ parameter gives the relation between the Nusselt height and L and ensures (when very small) that the derivation of the Benney equation is valid. As for δ, it is a parameter that appears after the nondimensionalisation and ensures that the perturbation has small amplitude compared to 1, the normalized Nusselt height.

We keep the term of the Benney equation with control (41) until order 1 in δ included. It gives a linear equation that we will use for the control:

21

$$\tilde{h}_{,t} = \left[-2\partial_x + (\frac{2cot(\theta)}{3} - \frac{8Re}{15})\partial_{xx} - \frac{1}{3Ca}\partial_{xxxx}\right]\tilde{h} + \left[\frac{1}{3}\partial_{xx}\right]\tilde{N}_s. \tag{43}$$

We study here the case

$$\tilde{N}_s = 0.$$

We decompose $\tilde{h}$ as

$$\tilde{h}(x,t) = \sum_{k\in\mathbb{Z}} c_k(t)e^{i\nu kx}.$$

with $\nu = \frac{2\pi}{L}$ as $\tilde{h}$ is L-periodic. So by differentiative with respect to t and isolating the Fourier coefficientwe, wehave $\mathbb{Z}$ number of ODEs:

$$c_{k,t}(t) = \lambda_k c_k(t). \tag{44}$$

Denoting for all integer k, $k_L = \nu k$, the λ_k can be written as

$$\forall k \in \mathbb{Z}, \lambda_k = (ik_L)^4(\frac{-1}{3Ca}) + (ik_L)^2(\frac{2}{3}cot(\theta) - \frac{8Re}{15}) - 2k_L i$$

$$= (\frac{8Re}{15} - \frac{2}{3}cot(\theta) - \frac{k_L^2}{3Ca})k_L^2 - 2k_L i.$$

Like in A.Thompson and al. paper [16], let us set

$$Re_0 = \frac{5}{4}cot(\theta). \tag{45}$$

and call it the unstable Reynolds number. The dispersion equation is then becomes

$$\lambda_k = -2ik_L + \frac{8}{15}\left(Re - Re_0 - \frac{5k_L^2}{8}\right)k_L^2. \tag{46}$$

The **stability** of the linear system is determined by a condition on the real part of the eigenvalues:

$$\mathcal{R}(\lambda_k) \leq 0.$$

$\mathcal{R}(\lambda_k) = P(\lambda_k^2)$ with P a polynomial of order 2 going to minus infinity at infinity. Hence, the unstable/diverging modes k verify

$$|k| \leq k_0 := \sqrt{Ca(\frac{8}{5}Re - 2cot(\theta))} = \sqrt{\frac{8Ca}{5}(Re - Re_0)}. \tag{47}$$

We see that if $Re < Re_0$, there is no unstable modes. Hence, having a larger Reynolds number would give more place to inertia and so more chance to have a chaotic flow. Therefore, we call Re_0 the unstable Reynolds number.

4 Numerical simulations

In this part of the report, we present the numerical scheme that we use to solve the Benney equation (41) on python. Then, we carry out different tests to evaluate its accuracy. All the system settings are in the python file *header.py* and the verifications are in the file *benney_eq_verif.py* in the Github repository. The solver is implemented in the file *solver_BDF.py* .

4.1 Description of the numerical framework

We code the simulations on python. We describe in this part of the report the numerical settings and the numerical schemes.

Physical variables. We list here the global variables that we use in the code and how we use them related to the physics of the system :

- System: L, T, θ

- Fluid characteristics: ρ_l, μ_l, γ

- Nusselt height and speed: h_N, U_N

The Buckingham's Pi theorem tells us that we essentially need 3 nondimensionalised groupings to describe all the physical variables. All the information can here be summarized in

$$Re = \frac{\rho_l U_N H_N}{\mu_l}, \quad Ca = \frac{mu_l U_N}{\gamma}, \quad U_N = \frac{\rho_l g h_N^2 sin(\theta)}{2\mu_l},$$

as U_N can have the same use as the Froude number $Fr = \frac{U_N}{\sqrt{\rho_l g}}$ to balance kinetic and gravitational energy if Ca and Re are fixed. However, it is obvious that we want to fix θ first and not define it from U_N as we want to have a vision of the system we're simulating.

We make the choice to be able to choose all the physical and system variables, and to deduce $h_N = \frac{Re\mu_l^2}{Ca\rho_l\gamma}$ and $U_N = \frac{\rho_l g h_N^2 sin(\theta)}{2\mu_l}$ from them. For the numerical simulations, we just need to ensure that the speed do not take nonphysical values and that

$$\epsilon = \frac{h_N}{L_x} \ll 1, \quad Re = O(1), \quad Ca = O(\epsilon^2). \tag{48}$$

The Model: steps and heigth. The model variables are :

$$N_x, N_t, dx = \frac{L}{N_x}, dt = \frac{T}{N_t - 1}, \tag{49}$$

23

i.e the space and time number of point and steps. The expression of dt and dx are different because we study a space periodic system so we discretize $[0, L_x - dx]$ with N_x points.

We try to have a relation between dx and dt that ensure a good balance between the space and time precision. We set the Courant-Friedrichs-Lewy (CFL) condition:

$$C = \frac{U_N dt}{dx} \leq C_{max} = 1. \tag{50}$$

We do that to ensure that the information in the space-time grid that we construct can transmit information throughout time faster than the speed of the numerical solution. We take C_{max} as said in the Wikipedia page of CFL condition . However, this condition was constructed for a simple advection partial differential equation where we know exactly the speed of the numerical solution. We took here the speed being the Nusselt speed without much confidence, and we indeed saw that it could lead to problematic values of dt. Indeed, U_N is very small so we would have few number of time points, giving a large dt. Therefore, we replaced that relation by

$$dt = min(dx, \frac{dx}{U_N C_{max}}), \tag{51}$$

which ensures that we have a decent time stepping precision.

We denote the matrix

$$(h_j^n)_{(n,j) \in [0, N_t-1] \times [0, N_x-1]} \in \mathcal{M}_{N_t, N_x} \text{ with } h(jdx, ndt) \approx h_j^n. \tag{52}$$

being the discrete numerical equivalent of the function $h : (x, t) \rightarrow h(x, t)$. We also note the horizontal vector at a fixed time

$$\underline{h}^n = (h_j^n)_{j \in [0, N_x-1]}.$$

At the border, we can check that

$$h_{N_t-1}^{N_x-1} = h((N_x - 1)dx, (N_t - 1)dt) = h(L - dx, T).$$

4.2 Description of the scheme

The Benney equation with control (41) has time and space derivatives, so we need a scheme to approximate the space derivative and another scheme for the time derivative. We could have taken the Fourier series of h to only study ordinal differential equation as we did with the KS equation (7). However, the non-linearities in the Benney equation (39) are far more complex than the Burgers non-linearities, which was already giving non trivial entanglement (the $F_j^{c,s}$), of the different Fourier coefficient of u. Therefore, we prefer to solve the equation with a time scheme and a space scheme.

We decide to take a **Backward Differentiation Formula (BDF)** for the time solving part. As for the space derivatives, we decide to use two methods separately :

finite difference and spectral methods.

Scheme for the time. As said above, we decide to use a BDF scheme (cf the
wikipedia page of BDF schemes).

An $N_{BDF} \in \mathbb{N}^*$ order BDF scheme can be written as an equation with unknown
$\underline{h}^{n+N_{BDF}}$ (implicit scheme in time) :

$$\underline{h}^{n+N_{BDF}} + \sum_{i=0}^{N_{BDF}-1} \alpha_{N_{BDF},i}\underline{h}^{n+i} = dtf(\underline{h}^{n+N_{BDF}}, t_{n+N_{BDF}}). \qquad (53)$$

Here, $(\alpha_{N_{BDF},i})_{1 \leq i \leq N_{BDF}}$ is the coefficients of the N_{BDF}-order BDF scheme, and f is
an operator that computes the part of the Benney equation without time derivatives.
f will be defined later either with finite difference or spectral methods.

Here, we consider $N_{BDF} \in [|1,6|]$ but not further, as the scheme do not work above
(cf again the wikipedia page: the scheme wouldn't be zero-stable which roughly means
that an arbitrary small perturbation can grow exponentially). We will make tests to
see which order to take for our experiments.

Two space schemes. We use a centered finite difference scheme for the space
derivative:

$$\begin{aligned}
h_{xxxx}(x_j, t_n) &= \frac{1}{dx^4}[h_{j+2}^{n+1} - 4h_{j+1}^{n+1} + 6h_j^{n+1} - 4h_{j-1}^{n+1} + h_{j-2}^{n+1}] \\
h_{,xxx}(x_j, t_n) &= \frac{1}{dx^3}[h_{j+2}^{n+1} - 3h_{j+1}^{n+1} + 3h_j^{n+1} - h_{j-1}^{n+1}] \\
h_{xx}(x_j, t_n) &= \frac{1}{dx^2}[h_{j+1}^{n+1} - 2h_j^{n+1} + h_{j-1}^{n+1}], \\
h_x(x_j, t_n) &= \frac{1}{2dx}[h_{j+1}^{n+1} - h_{j-1}^{n+1}].
\end{aligned} \qquad (54)$$

The precision of the scheme is fixed by the least precise approximation, which would
be here the one of h_x. As we take a centred scheme, we have an **error in $O(dx^2)$** and
not an error in $O(dx)$, which would have arisen with a forward or backward scheme.

We denote $mat_{FDper}(N_x, [a, b, c, d, ..])$ (matrix for a periodic finite difference scheme)
a matrix in $\mathcal{M}_n$ with only a in its diagonal, b in its subdiagonal, c in its supdiagonal,
d in its 2nd subdiagonal etc... The terms in the sub/sup diagonals are extended as it's
a periodic problem. For example,

$$mat_{FDper}(N_x, [3, -1, -3, 0, 1]) = \begin{pmatrix} 3 & -3 & 1 & \cdots & \cdots & 0 & -1 \\ -1 & 3 & -3 & 1 & & \ddots & 0 \\ 0 & -1 & 3 & -3 & 1 & \cdots & 0 \\ & \ddots & \ddots & \ddots & \ddots & & \\ 0 & \cdots & 0 & -1 & 3 & -3 & 1 \\ 1 & 0 & \cdots & 0 & -1 & 3 & -3 \\ -3 & 1 & \cdots & \cdots & 0 & -1 & 3 \end{pmatrix}. \tag{55}$$

Hence, in python (with a little change in the code notation):

```
mat_DF_x = mat_FD_periodic(N_x, [0, -1, 1])/(2*dx)
mat_DF_xx = mat_FD_periodic(N_x, [-2, 1, 1])/dx_2
mat_DF_xxx = mat_FD_periodic(N_x, [3, -1, -3, 0, 1])/dx_3
mat_DF_xxxx = mat_FD_periodic(N_x, [6, -4, -4, 1, 1])/dx_4
```

As we suppose h to be L-periodic in space, we also test a <u>spectral method</u> as a spatial scheme. Let us decompose h into its Fourier series:

$$h(x, t) = \sum_{n \in \mathbb{Z}} c_n(t) e^{inx},$$

with

$$\forall n \in \mathbb{Z}, \quad c_n(t) = \frac{1}{2\pi} \int_{-\pi}^{\pi} h(x, t) e^{-inx} dx.$$

Hence

$$\forall d \in \mathbb{N}, \quad \frac{\partial^d h}{\partial x^d} = \sum_{n \in \mathbb{Z}} (in)^d c_n(t) e^{inx}$$

Numerically, we use the *numpy.fft.rfft* function that computes the c_n for $n \in [|0, N_x/2|]$ as $c_{-n} = \bar{c}_n$ as h is real.The *numpy.fft.irfft* computes the inverse Discrete Fourier Transform.

Therefore, we compute the derivatives this way:

```
h_x = np.fft.irfft( (1j *fq_tab)*np.fft.rfft(h_arr))
h_xx = np.fft.irfft( (1j *fq_tab)**2*np.fft.rfft(h_arr))
h_xxx= np.fft.irfft( (1j *fq_tab)**3*np.fft.rfft(h_arr))
h_xxxx= np.fft.irfft( (1j *fq_tab)**4*np.fft.rfft(h_arr))
```

with *fq_tab* being the table of all the frequencies used by the Fast Fourier Transform. We prefer to use that method over the finite difference one as it is <u>significantly faster</u> (at least 3 or 4 times faster), surely due to the efficiency of the fft package. However, in opposite to the finite difference method, we do not know the precision of the scheme.

Nevertheless, the finite difference scheme will still be useful as we will compare both method to evaluate the accuracy of the numerical scheme.

Total scheme. As said in the BDF scheme description, we have to solve a non linear system at each time step. In the code, we call 'F_time' (resp. 'F_space') the function which computes the BDF part of the scheme (i.e the left part of (53)) using all the previous $(\underline{h}^{n+1-i})_{i\in[|1,N_{BDF}|]}$ (resp. the function that computes the space derivatives with the current height to find $\underline{h}^{n+1}$). We finally solve this implicit non linear problem in $\underline{h}^{n+1}$ by interpreting it as a <u>root finding problem</u> of a function $f : \mathbb{R} \to \mathbb{R}^{N_x}$. The problem to solve is then

$$\boxed{\text{Find } \underline{h}^{n+1} \in \mathbb{R}^{N_x}, \quad F_{time}(\underline{h}^{n+1}, (\underline{h}^{n+1-i})_{i\in[1,N_{BDF}]}) + F_{Space}(\underline{h}^{n+1}) = 0.} \tag{56}$$

We use the **scipy.optimize.root** function which chooses a root finding solver among many and uses it. The function outputs each time if it converges or not with the evaluation of the root so it allows us to control the convergence at each time steps by watching if the value is close to 0 or not.

4.3 Verification and validation of the schemes

In this section, we check the validity of the numerical schemes. More concretely, we test the finite difference and spectral methods separately, and we also compare them based on the time and space stepping and BDF order N_{BDF}. Finally, we check some physical properties.

We denote
$$h_{FD}^{(N_x,N_{BDF})}, h_{Sp}^{(N_x,N_{BDF})}, h^{(N_x,N_{BDF})}, \tag{57}$$

the numerical result of the algorithm described above with a Finite Difference (resp. Spectral, resp. not precised) method, with a number of space point N_x (the number of time point N_t can be deduced with (51)), and a BDF method of order N_{BDF}.

We want to test our schemes on growing regimes and not dampening one as we will compare the schemes with the last time evaluation. We take these parameters for all the verifications :

$$\boxed{T = 160, L = 30, Re = 5, Ca = 0.01, \theta = \frac{\pi}{3}, \delta = 1.10^{-3}} \tag{58}$$

with initial conditions

$$\boxed{\underline{h}^{0,(N_x,N_{BDF})} = \delta sin(k\nu x), \quad k = 1.} \tag{59}$$

With these parameters, we verify the conditions (48). Moreover, the critical wave number (47) $k_0 \approx 1.2$ here so taking the first mode k=1 gives us a growing regimes

27

according to the linear theory, which was indeed observed in the simulations. Finally, we took δ small enough and T large enough so that we can have the final amplitude of the system very large compared to δ without the scheme to blow up (which happens for larger δ). For example, with these parameters, we know that the numerical scheme get stuck at $t \approx 180$ (we tested with $N_x = 512$ and $N_x = 1024$) so we took T a bit lower than that to have a significant final amplitude.

BDF scheme benchmarking We solve numerically equation (33) for different orders of schemes and display the different dynamics of the height on a video which can be found on the Github page. We didn't make use quantitative criteria (like norm analysis) and just judged by the visible difference in the dynamics. We tried that for $N_x \in \{128, 256, 512, 1024\}$.

We find that all the orders give close dynamics as of $N_x = 512$ except for $N_{BDF} = 1, 2$. We can see in figure 9 and (10) at the final time t=T at $N_x = 128$ and $N_x = 512$ and $N_x = 1024$ with the Finite Difference method (the results are exactly the same with the spectral method). We notice that the 2 first orders are not precise at all, the third order takes too large values, and that the fourth, fifth, and sixth order are quite close too each other. For $N_x = 1024$, we see in (10) that the orders 3, 4, 5 and 6 are quite close at the final time with a peak at the normalized height 1.3. It seems that order 3 to 6 are quite similar for $N_x = 1024$, same for the order 4 to 6 for $N_x = 512$.
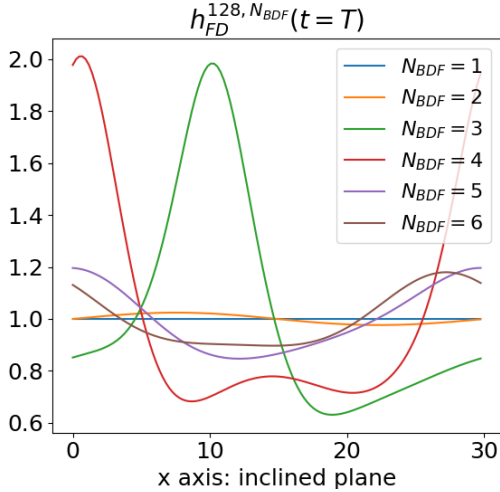

Figure 7: $N_x = 128$

Figure 8: $N_x = 512$

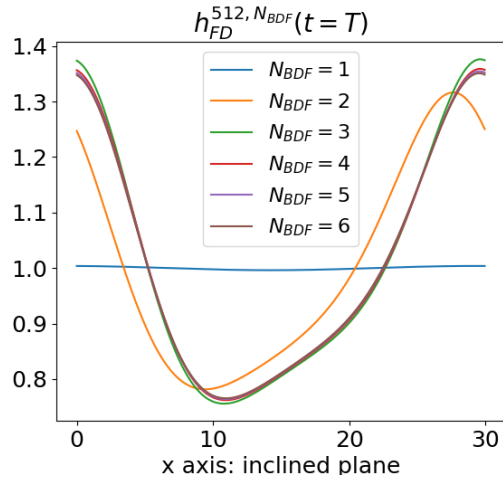Figure 9: Plot at the final time of $h_{FD}^{N_x, N_{BDF}}(t = T)$ with $N_{BDF} \in \{1, 2, 3, 4, 5, 6\}$ and fixed space step. The case $N_x = 128$ gives very different solution for different N_{BDF} whereas we can make out a common behaviour among the schemes, except $N_{BDF} = 128$ for the case $N_x = 512$.

From the results of figure 9, for the control experiments that we will carry on later,
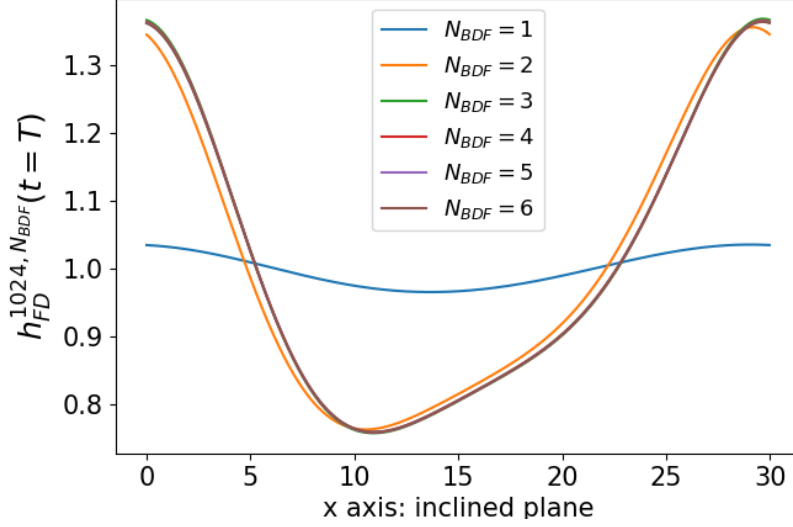
Figure 10: Plot of $h_{FD}^{1024,N_{BDF}}(t = T)$ for $N_{BDF} \in \{1, 2, 3, 4, 5, 6\}$. We observe that the third, fourth, fifth and sixth order BDF schemes are quite close. The second order is closer of the higher order compared to lower N_x. The $N_{BDF} = 1$ solution seems to be slightly better than the one obtained with lower N_x.

we choose to take

$$\boxed{N_x = 512}, \tag{60}$$

as $N_x = 1024$ is quite long to compute (1200s for the spectral scheme and 10000s for the Finite Difference scheme). We will choose N_{BDF} with the next study of the convergence of the schemes.

Study of the Convergence scheme convergence We solve numerically the equation to find $h^{(N_x, N_{BDF})}$ for different time steps, then we compute L^2 and L^∞ differences to the methods at the final time. We set the maximum number of points as

$$N_x^{max} = 1024.$$

We take that specific number because it was high enough to have good results and can be divided $\{128, 256, 512\}$ so we won't need to make any interpolation when we do the difference between the arrays (which do not have the same shape).

So what we compute is

$$||h^{(N_x^{max}, N_{BDF})}(T) - h^{(n, N_{BDF})}(T)||_{L^p([0,L])} \tag{61}$$

with $p \in \{2, +\infty\}, n \in \{1024/i, i \in \{2, 4, 8\}\} = \{512, 256, 128\}$. We test with the settings (58) which give an exponentially growing regime. The fact that the system forms an exponentially growing wave allows us to probably have all the discrepancy during the transitional regime amplified at the final time. Therefore, it justifies in a sense why
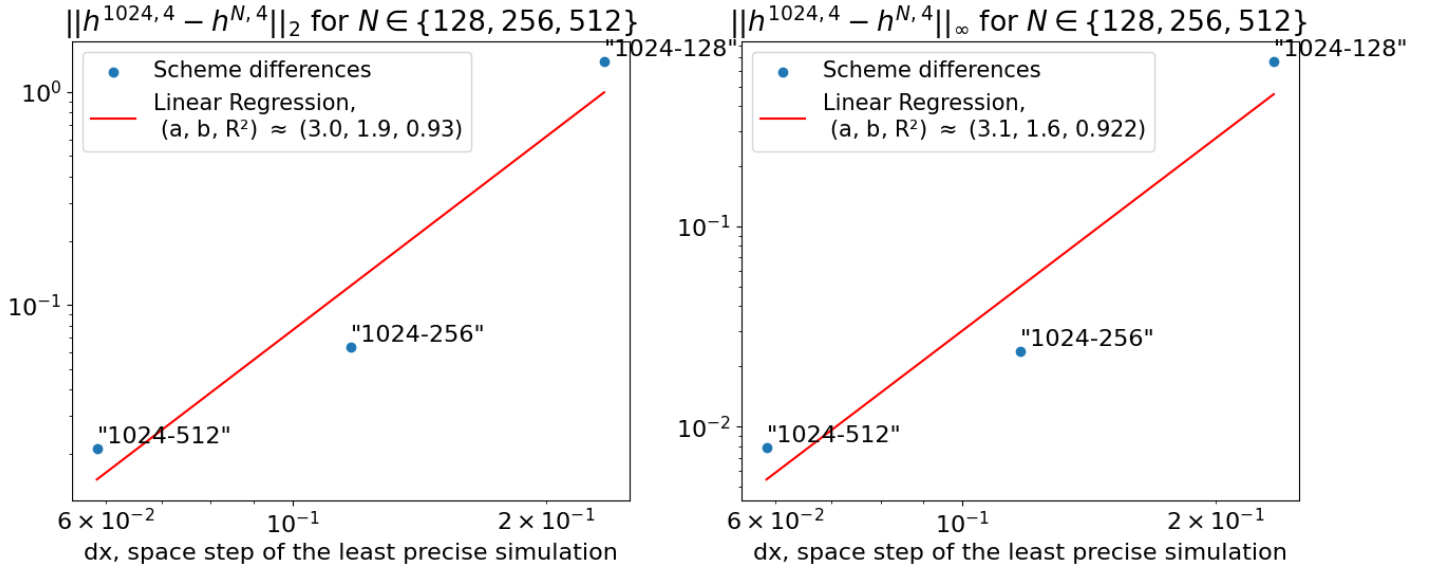
29

Figure 11: Plot in a log-log graph of $||h_{Sp}^{1024,4}(T) - h_{Sp}^{N_x,4}(T)||_{L^p}$, for $N_x \in \{128, 256, 512\}$ and $p \in \{2, +\infty\}$. We see that the L^2 and L^∞ errors between the schemes and the most precise scheme are decreasing with an exponential behaviour. To highlight this exponential decrease, we drew the linear regression of $\log\left(||h_{Sp}^{1024,4}(T) - h_{Sp}^{N_x,4}(T)||_{L^p}\right)$.

we test the numerical scheme this way[4].

Among the $12 = 6 \times 2$ graphs (one for each methods and for each N_{BDF}) that we computed, we find that difference in L^2 and L^∞ norm are decreasing exponentially, with a higher rate at $N_{BDF} = 3$ and 4. We show in figure 11 a plot of (61) for the spectral method with $N_{BDF} = 4$.

Taking into account the observations in figures 9 and 11, we choose

$$\boxed{N_{BDF} = 4, \quad N_x = 512} \tag{62}$$

for the experimentation in the upcoming control part.

Comparison of the schemes. We also compared the finite difference and spectral scheme to check if would give the same results. We obtain a good matching of the schemes, with increasingly small errors with smaller space steps dx for $N_{BDF} \geq 3$. In figure 12, with $N_x = 512$ and $N_{BDF} = 4$, we have the error at between 10^{-2} and 10^{-3} which is very small compared to the final amplitude of the regime 3.10^{-1}.

Physical properties. We check here some physical properties.

---

[4]We test exponentially growing regimes so discrepancies during the transitional regime would be probably amplified at the final time.
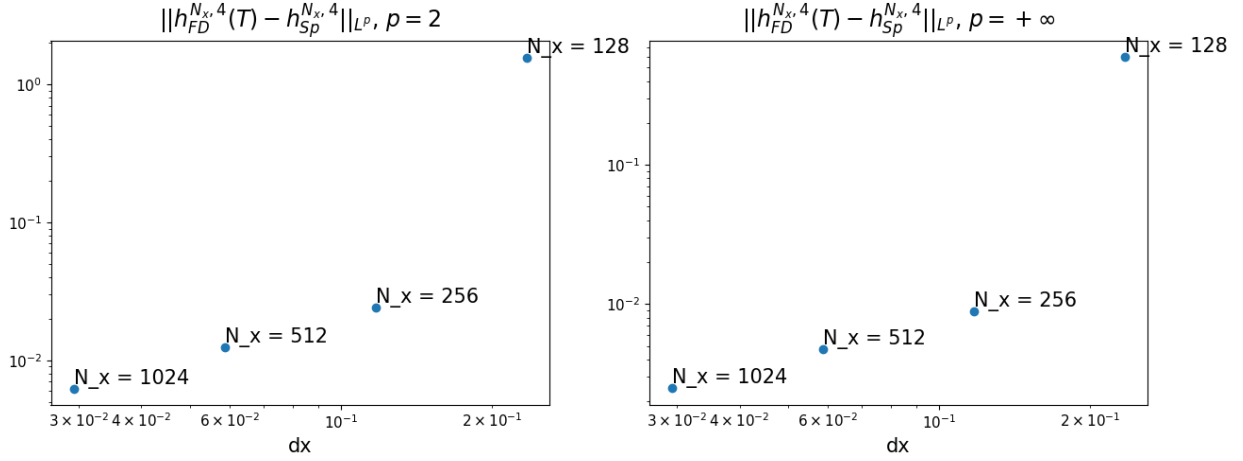
Figure 12: Plot of $||h_{FD}^{N_x,4}(T) - h_{Sp}^{N_x,4}||_{L^p}$ with $N_x \in \{128, 256, 512\}$ and $p \in \{2, +\infty\}$. We see that the L^∞ norm of the difference when $N_x = 512$ is around 1.10^{-2} and 1.10^{-3} which seems to be satisfactory for a final state of amplitude 3.10^{-1}.

The mass of the whole fluid is $M = \int_0^L \rho_l(x,t)h(x,t)dx$ and as $\rho_l(x,t) = \rho_l$ is uniform and static, we call "mass" the quantity

$$M_h := \int_0^L h = \frac{M}{\rho_l}. \tag{63}$$

Integrating the Benney equation (39), and deriving with respect to t, we have that:

$$M_{,t} = \int_0^L h_{,t}dx = -\int_0^L q_{,x}dx = -\int_0^L [q_{,x}^B + q_{,x}^{control}]dx$$
$$= \int_0^L (h_{,x}h^2 N_{s,x} + \frac{h^3}{3}N_{s,xx})dx = \int_0^L [\frac{h^3}{3}N_{s,x}]_{,x}dx,$$

where we used the Benney equation to introduce the flux q. We decomposed q into the Benney part (without the N_s) and control part : $(q^B, q^{control})$ and we supposed that the Benney equation without Control conserves mass, which is the case, numerically at least. Finally, as h is L-periodic:

$$M_{,t} = \frac{h^3(0,t)}{3}(N_{s,x}(L) - N_{s,x}(0)). \tag{64}$$

Therefore, the mass variation depends on the discontinuity gap of the derivative. We check this equality numerically by using actuators of the form

$$N_s : x \in [0,L] \mapsto \sum_{j=1}^k u_j(t)d(x - x_j),$$

31

with k being the number of air jets and d a gaussian with a significant standard deviation (i.e a relatively flat gaussian). We see indeed that the variation rate of the height follows to the analytical rate (64) with very small relative error ($< 1\%$).

We also checked other qualitative properties. For example, if we put a higher air jet intensity, we will have deeper trough, or, for the same intensity, if we increase the slope angle θ, we will have a bigger bump. We also played a bit with the viscosity and surface tension coefficient μ_l and γ and saw that increasing surface tension would lead to flatter bump which seems to be physically relevant as surface tension tends to keep the liquid flat.

5 Control

Now that we set up the numerical scheme, we use the linearized Benney equation (43) in order to use different type of control to stabilize the film height towards the Nusselt solution. We will present Feedback proportional control and state Feedback Linear Quadratic Regulator (LQR) control strategies. None of these strategies put any constraints on the sign of the control, which has to be positive in our case (blowing air jets), so we also test if the positive part of these control can stabilize the film. Finally, these strategies do not give any proof that the height and the control stay positive, which is called a positive control system. Hence, we construct an asymptotically stable positive control scheme and try to make it work numerically. All the control experiments are implemented either in the file *main_benney_eq_Ctrl.py* or in *Control_file.py* that are available in Github repository.

5.1 Continuous and discrete Control system

In this section, we present the continuous and discrete linear control system with feedback control and link it to the falling liquid system that we study.

5.1.1 Feedback control: an exponential dynamical matrix system

We want to stabilize the fluid towards the normalized Nusselt solution h(x,t) =1. To do that, we want to use a linear control strategy framework of the form

$$\begin{cases} x_{,t} = \mathcal{A}x + \mathcal{B}u, & y = \mathcal{C}x \\ \qquad\qquad x(t=0) = x_0 \end{cases} \tag{65}$$

with $x, u, y \in L^2(\mathbb{R}_+, L^\infty([0,L], \mathbb{R}))$ the state of the system, the control, and the output (or observations) of the system respectively. $\mathcal{A}, \mathcal{B}$, and $\mathcal{C}$ are bounded linear operators that describe respectively the control-free dynamical system, the control impact on the system, and how much we can observe the state x.

The discrete and finite dimensional equivalent system which is more tractable for our numerical approach is

$$\begin{cases} x_{,t} = Ax + Bu, & y = Cx \\ \qquad\qquad x(t=0) = x_0 \end{cases}, \tag{66}$$

with $\forall t \geq 0, x(t) \in \mathbb{R}^n$, $u(t) \in \mathbb{R}^k$, and $y(t) \in \mathbb{R}^n$, $A \in \mathcal{M}_n(\mathbb{R})$, $B \in \mathcal{M}_{n,k}(\mathbb{R})$, $C \in \mathcal{M}_n(\mathbb{R})$. Here, $n, k \in \mathbb{N}^*$ are respectively the number of space discretization the of air jets that we will use.

We choose to take

$$C = I_d, \tag{67}$$

which means that we have a full observation of our state, which is a strong assumption. Indeed, as we will see later in the next section 5.1.2, the state x will be the height of the film. Having full observation means that we can, at all time, measure exactly the height. These kind of assumptions can be realistic with laboratory equipment, like in [4] where they use precise optical measurements and vision algorithms to measure accurately the height of the liquid film. However, in an industrial framework, it is not sure that this hypothesis is still realistic. It becomes even more difficult in the case of the Weighted Residuals model, another reduced-order model of the Navier-Stokes equations, as one would have to measure exactly the height h and the flux q.

As we want to use a feedback control strategy, the control is of the form

$$u = Ky = Kx, \quad K \in \mathcal{M}_{k,n}. \tag{68}$$

Hence, the system can be rewritten as

$$\begin{cases} x_{,t} = (A + BK)x \\ \quad x(t = 0) = x_0 \end{cases}, \tag{69}$$

which is an exponential system of solution

$$s : t \mapsto e^{(A+BK)t} x_0.$$

As we want the system to be stable, all the eigenvectors of the matrix A+BK need to have a negative real part so that their exponential evaluation vanishes. We call these matrices Hurwitz matrices. Therefore, the problem can be finally rewritten as a pole placement problem:

$$\boxed{\text{Find } K \in \mathcal{M}_{n,k}, \quad \forall v \in Sp(A + BK), \Re(v) < 0} \tag{70}$$

or

$$\text{Find } K \in \mathcal{M}_{n,k}, \quad A + BK \text{ is Hurwitz,} \tag{71}$$

with Sp the notation for spectrum and $\Re$ for the real part of a complex number.

5.1.2   Link with the falling liquid system

We link here the linear control framework with our physical system..
    We take

$$\tilde{h} = \frac{h - 1}{\delta} \tag{72}$$

34

the "zoomed" perturbation from the perturbed normalized height (42). We recall the linearized Benney equation with air jet control (43):

$$\tilde{h}_{,t} = \left[-2\partial_x + (\frac{2cot(\theta)}{3} - \frac{8Re}{15})\partial_{xx} - \frac{1}{3Ca}\partial_{xxxx} \right] \tilde{h} + \left[\frac{1}{3}\partial_{xx} \right] \tilde{N}_s.$$

We take a (scaled) normal stress as a sum of k controlled actuators which represent the air jet:

$$\tilde{N}_s = \sum_{j=1}^{k} u_j(t)d(x - x_j), \tag{73}$$

with

$$\forall x \in [0, L], \quad d(x) = A exp\left(\frac{cos(\nu x) - 1}{\omega^2} \right). \tag{74}$$

A is here chosen such that $\int_0^L d = 1$. $\nu = \frac{L}{2\pi}$ and ω to be chosen later in the program (`omega_NS = 0.1`).

So the total equation becomes

$$\tilde{h}_{,t} = \mathcal{A}\tilde{h} + \mathcal{B}u$$

with

$$u = (u_j)_{j \in [\![1,k]\!]} \in L^2(\mathbb{R}_+, \mathbb{R})^k,$$

$$\mathcal{A} = -2\partial_x + (\frac{2cot(\theta)}{3} - \frac{8Re}{15})\partial_{xx} - \frac{1}{3Ca}\partial_{xxxx},$$

and

$$\mathcal{B} : \begin{pmatrix} u \mapsto \left(t \to \frac{1}{3}\sum_{j=1}^{k} u_j(t)d_{xx}(. - x_j) \right) \\ L^2(\mathbb{R}_+, \mathbb{R})^k \to L^2(\mathbb{R}_+, L^\infty([0, L], \mathbb{R})) \end{pmatrix}.$$

We have now linked the Benney system to the continuous linear control model (65) with the same notations, except for the state x which is here $\tilde{h}$. We only have a little difference with the control u as we introduced a specific form for the control, so the functional space is a bit different, but it will not affect the discrete problem.

The discrete system. We discretize the system and have N_x numbers of ODEs. We also add the feedback control with full observations:

$$\boxed{\frac{d\tilde{h}}{dt} = A\tilde{h} + Bu, \quad u = K\tilde{h}.}$$ (75)

We directly have the similarity with the discrete linear control framework (66) with

$$n \approx N_x, x \approx \tilde{h} \in \mathbb{R}^{N_x}, A \in \mathcal{M}_{N_x}, B \in \mathcal{M}_{N_x,k}, \text{ and } C = I_d \in \mathcal{M}_{k,N_x}.$$

We denote

$$u^i \in \mathbb{R}^k, \tilde{h}^i \in \mathbb{R}^{N_x}, \quad i \in [|1, N_t|]$$ (76)

the control and centred height at time $t_i = i \times dt$ respectively.

The matrices A and B are constructed with a centred finite difference scheme, so using the notations of the finite difference matrices, the matrix A is :

$$\boxed{\begin{aligned} A = {} &\alpha_1 mat_{FDper}(N_x, (0, -1, 1)) + \alpha_2 mat_{FDper}(N_x, (-2, 1, 1)) \\ &+ \alpha_3 mat_{FDper}(N_x, (6, -4, -4, 1, 1)), \end{aligned}}$$ (77)

with

$$\alpha_1 = \frac{-2}{2dx}, \alpha_2 = \frac{1}{dx^2}\left(\frac{2cot(\theta)}{3} - \frac{8Re}{15}\right), \alpha_3 = \frac{-1}{3Cadx^4}.$$

The matrix B is

$$\boxed{B = (\frac{1}{3}d_{xx}(x_i - x_j))_{(i,j)\in[|1,N_x|]\times[|1,M|]} \in \mathcal{M}_{N_x,k}(\mathbb{R})}$$ (78)

as

$$\forall (i,l) \in [|1, N_x|]\times[|1, N_t|], \quad \sum_{j=1}^{k} B_{ij}u_j^l = (Bu^l)_i = (\frac{1}{3}\partial_{xx}N_s(l\times dt))_i = \frac{1}{3}\sum_{j=1}^{k} u_j^l d_{xx}(x_i - x_j).$$

5.2 LQR Control

In this section, we implement Linear Quadratic Regulator (LQR) Control. As its name suggests it, it is a type of linear control linked to a quadratic function. This function will be here a quadratic cost that we will introduce later. We will see that LQR control succeeds to stabilize the Benney system. Then, as we want blowing only air jets, we take the positive part of that control at each time steps. We find that despite being less efficient then the classic LQR control, the positive part of the LQR control stabilizes successfully the Benney system. Then, we retrieve the speed of convergence of the LQR control by multiplying the control by a scalar $\zeta_+ = 2$, which also leads to increase the cost of the control compared to the classic LQR.

5.2.1   LQR Control and Riccati equation

We first deal with the continuous system and introduce the cost function

$$\kappa(u) = \int_0^{+\infty} \int_0^L \left[\beta(\tilde{h}(x,t) - \xi(x))^2 + (1-\beta)\tilde{N}_s(x,t)^2 \right] dx dt. \tag{79}$$

It is a cost functional whose weight β translates the importance given to the distance between the system state x to a goal state $\xi \in L^2([0,L], \mathbb{R})$ compared to the quadratic cost of the control $\tilde{N}_s$. As we want to stabilize the system towards the Nusselt solution $(\tilde{h} = 0)$, we take naturally

$$\forall x \in [0,L), \quad \xi(x) = 0.$$

Let us define

$$D = (d(x_i - x_j))_{(i,j) \in [|1,N_x|] \times [|1,k|]}$$

with d the shape function of the air jet actuators. We then define the discrete counterpart of the continuous cost κ:

$$\boxed{c = \int_0^{+\infty} (\tilde{h}^T Q \tilde{h} + u^T R u) dt}, \tag{80}$$

with

$$R = (1-\beta)\frac{L}{N_x} D^T D \quad \text{and} \quad Q = \beta\frac{L}{N_x} I_{N_x}. \tag{81}$$

We justify this definition of c with the following approximations of integrals by their Riemann sums (rectangle method):

$$\beta \int_0^L \tilde{h}^2(x,t)dx \boxed{\approx} \frac{L}{N_x} \sum_{i=1}^{N_x} \tilde{h}^2(x_i,t) = \beta\frac{L}{N_x}\tilde{h}^T\tilde{h} = \tilde{h}^T Q \tilde{h}$$

and

$$(1-\beta)\int_0^L N_s^2(x,t)dx = (1-\beta)\int_0^L \left(\sum_{j=1}^M u_j(t)d(x-x_j)\right)^2 dx$$

$$\boxed{\approx} (1-\beta)\frac{L}{N_x}\sum_{i=1}^{N_x}\left(\sum_{j=1}^M u_j(t)d(x_i-x_j)\right)^2$$

$$= \sum_{1 \leq j,k \leq M} u_j(t)u_k(t)\left((1-\beta)\frac{L}{N_x}\sum_{i=1}^{N_x} d(x_i-x_j)d(x_i-x_k)\right)$$

$$= \sum_{1 \leq j,k \leq M} u_j(t)u_k(t)R_{j,k} = U^T R U.$$

The Riccati equation. We now present how we find the optimal control associated to the discrete cost c by solving a matrix equation. We know from [7] (part 3.2) for

37

example, that there exists a symmetric positive semi-definite matrix P solution to the problem

$$\text{Find } P \in \mathcal{M}_{N_x}, \quad 0 = A^T P + PA + Q - PBR^{-1}B^T P, \tag{82}$$

we can build a gain matrix of this form:

$$K = -R^{-1}B^T P. \tag{83}$$

The equation (82) is known as the Continuous Algebraic Riccati Equation (CARE). At the opposite of [7], we do not use a specific method to solve this equation and rather use the python library *python-control* with the function `control.lqr`. Moreover, we do not check the existence of a solution, but let us remark that if the system (A, B) is controlable, R is positive definite and Q semi-positive definite, then there exists one and only minimizer of the cost functional c which solves the Riccati equation because c would be stritly convex with respect to the cost $\tilde{N}_s$. Here, R and Q are obviously positive semi-definite and we checked numerically that R is positive definite.

5.2.2 Numerical experiment

We now try to stabilize the growing regime (58) with LQR control. We test classic LQR control first, which stabilizes efficiently the system. Then, we try to apply only the positive part of the LQR control, to mimic blowing only air jets. We find that this control also stabilizes the system, but is less efficient. We finally 'cheat' a little by multiplying the positive control by a constant $\zeta_+ = 2$, which improves the dampening rate but with negative effect on the cost.

Classic LQR Control. We implement the LQR control by solving the Continuous Algebrai Riccati Equation (CARE), as described at the end of the previous section. We test several weight parameters (every 5% of β) [5] to observe how this parameter affects the stabilization of the system, but also the total quadratic cost of the control. Here, we do not take into account the shape functions of the actuators and just look at the amplitudes as we just want to compare the cost

$$\kappa_u = \int_0^T \int_0^L u^2 dx dt \tag{84}$$

obtained with different values of β, or rather its numerical counterpart:

```
quad_cost_ctrl = np.sum(amplitudes_spectral**2)*dx**2*dt**2.
```

Here, *"amplitudes_spectral"* is the array of the amplitudes of the shape function (i.e $(u_j^i)_{(i,j)\in[|1,N_t|]\times[|1,k|]}$ in (76)) with a spectral method.

---

[5]Let us precise that the program do not find a solution for Riccati equation for some values of β like 0.1 or 0.5. Hence, some values of β like 0.05 or 0.25 do not appear in the tests.
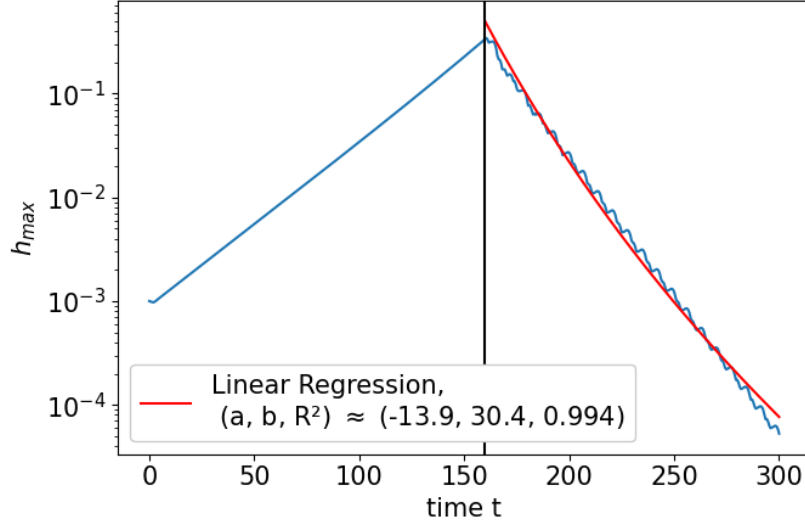
Figure 13: Semi $\log_{10}$ plot of $h_{max}(t) := max_{x \in [0,L)}|h(x,t) - 1|$ with a LQR control strategy of parameter $\beta = 0.95$, and a spectral scheme of parameter $N_x = 512$ and $N_{BDF} = 4$. We let the perturbation grow exponentially until $t = 160$, then we applied the LQR control which stabilized exponentially the system. The linear regression of a dampening rate of 14.0 obtained by a linear regression of $\log(h_{max})$ after the activation of the control gave a dampening rate of 14.0.

We consider that the system is stabilized when its maximal amplitude is lower than $\delta = 1.10^{-3}$, the amplitude of the initial perturbation. We take

$$T_{start} = 160, \quad T = 300, \tag{85}$$

the starting time of the control (to let the perturbation grow until a sufficient large state) and the total time of the simulation to let the time to the control to stabilize the system. The control stabilizes exponentially the system, as we can see in figure 13. We present in (2) the cost for different β.

We see that κ_u and $max_{\substack{1 \leq i \leq N_t \\ 1 \leq j \leq k}} |u_j^i|$ are increasing with β, which is expected as we lower the weight on the cost of the control to have a better stabilization. Let us also notice that the result does not really change depending on β, except for $\beta = 0.95$ where we have a significant increase of the damping rate d_r.

The LQR control stabilizes well the Benney system, and the videos of the controls can be seen in the Github repository. As said before, this result is not sufficient as we used blowing and suction air jets and we want to use blowing-only air jets control.

Positive part of LQR Control. Now, we take the positive part of the LQR

39

Table 2: LQR Control: Array of the cost κ_u and dampening rate d_r with different values of β each 5% when the solver finds a solution to the Riccati equation.

β	0.2	0.3	0.35	0.4	0.5
κ_u	3.0284	3.0086	3.0323	3.0340	3.0385
d_r	10.5	10.5	10.5	10.5	10.6
$\max_{\substack{1 \le i \le N_t \\ 1 \le j \le k}} |u_j^i|$	7.2761	7.2908	7.2999	7.3104	7.3376
β	0.55	0.65	0.75	0.8	0.95
κ_u	3.0415	3.0501	3.0654	3.0789	3.2743
d_r	10.7	10.8	11	11.2	13.9
$\max_{\substack{1 \le i \le N_t \\ 1 \le j \le k}} |u_j^i|$	7.3556	7.4066	7.4966	7.5735	8.6401

control to construct a blowing only air jet control, i.e

$$u_{pos} = |-R^{-1}B^T P\tilde{h}|^+ = |Ku|^+, \tag{86}$$

P being the solution of the continuous algebraic Riccati equation (82).

We find that the system stabilizes also exponentially but around 3-4 times slower, with the dampening rate d_r being around 3 in the positive part case against 14 in the normal case. We tried to carry out simulations with $T = 1000$ in order to see the decrease of the amplitude until the end. However, the configuration given by (62) do not seem to be enough as the system Benney system with variables (58) blocks before $t = 160$ (the time on when the system was not blocking with $N_x = 512$ and $N_x = 1024$), which seems to mean that the number of time (here $N_t = N_x = 512$) and steps point isn't enough for T=1000.

From a physical point of view, it was expected that the control will be less efficient as we remove half of the energy of the normal LQR control. That is why we changed the control by taking the positive part of the control times a coefficient :

$$u_{pos} = \zeta_+ |Ku|^+, \quad \zeta_+ = 2. \tag{87}$$

We took $\zeta_+ = 2$ to compensate the lack of energy, as said before. Of course, the compensation is not exact as we do not have exactly half of the energy taken by the blowing and half from the suction [6]. As we can see in figure 14, we retrieve the dampening rate of the initial LQR control method. Moreover, as expected, the cost κ_u is higher than the classical LQR method, of around $\frac{4-3}{3} = 33\%$, as we can see in array 3. Finally, the maximal values of the control u have doubled, which might mean that the control blows the same way as the normal LQR control because we have compensated in a way the removed suction mechanism with more blowing by the mean of the parameter $\zeta_+ = 2$.

---

[6]We could have measured that total amount of energy used for sucking, and then put it directly on ζ_+ but we didn't have the time to do so.

Table 3: Positive part of LQR Control: array of κ_u and d_r for varying β and $\zeta_+ = 2$.

β	0.2	0.3	0.35	0.4	0.5
κ_u	4.2887	4.2887	4.2956	4.2986	4.3065
d_r	10.9	10.9	10.9	11	11
$\max_{\substack{1 \leq i \leq N_t \\ 1 \leq j \leq k}} \left\|u_j^i\right\|$	14.2863	14.3168	14.3355	14.3573	14.4136
β	0.55	0.65	0.75	0.8	0.95
κ_u	4.3117	4.3266	4.3532	4.3762	4.6957
d_r	11.1	11.2	11.4	11.6	14.2
$\max_{\substack{1 \leq i \leq N_t \\ 1 \leq j \leq k}} \left\|u_j^i\right\|$	14.4509	14.5565	14.7431	14.9029	17.0068

In conclusion, we found a method that stabilizes exponentially the Benney system with blowing only air jets. However, a more detailled study of the cost should be made to find better values of ζ_+ that would give cheaper cost and higher dampening rate.

Finally, in the same spirit as in the section III/D of [16] but here with the Benney system and not Weighted Residuals, let us underline that we do not fully stabilize the Benney system, but just bring it to another state. Therefore, if we stop the control when the amplitude is small but with the system being in a growing exponential mode (like the initial condition (58)), the system will just grow up exponentially again.

5.3 Proportional Control

We noticed in the videos showing the dynamics of the liquid that the actuators seemed to have a behaviour similar to the one of proportional control (sucking when there is a trough, blowing when there is a crest). Therefore, we lean on proportional control, a simpler control mechanism, to see if the complexity of the LQR control was needed to have good results. We implement the proportional control strategy and compare its results to the one obtained with LQR control.

5.3.1 The linear theory

We now do proportional control, i.e control of the type

$$\tilde{N}_s = \alpha\tilde{h} = \alpha\frac{h-1}{\delta}, \quad \alpha > 0. \tag{88}$$

Concretely, $\tilde{N}_s \geq 0$ when $\tilde{h} \geq 0$ and $\tilde{N}_s \leq 0$ when $\tilde{h} \leq 0$. So we push when there is a crest and suck when there is a trough, which is a quite basic and intuitive strategy to follow to flatten the fluid.

We do exactly the same type of analysis as [16] where they used proportional control with fluid blowing and suction actuation. To find a criterion on α, we make a stability analysis on linearized Benney equation (43) and take the feedback form of $\tilde{N}_s$ (88):
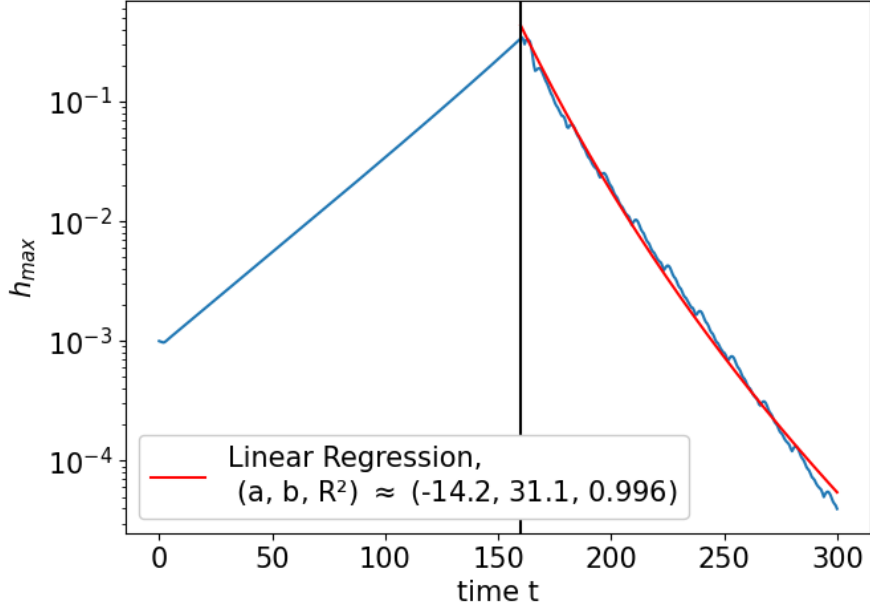
Figure 14: Semi $\log_{10}$ plot of $h_{max}(t) = max_{x \in [0,L)}|h(x,t) - 1|$ with a LQR control strategy of parameter $\beta = 0.95$ truncated to its positive part and multiplied by $\zeta_+ = 2$. The spectral numerical scheme is set up with $N_x = 512$ and $N_{BDF} = 4$. We let the perturbation grow exponentially until $t = 160$, then we applied the control which stabilized exponentially the system. We retrieve the same dampening rate as the previous LQR control in figure 13 but the strategy is more expensive, as we can see by comparing tables 2 and 3.

$$\tilde{h}_{,t} = \left[-2\partial_x + \left(\frac{8}{15}(Re_0 - Re) + \frac{\alpha}{3} \right) \partial_{xx} - \frac{1}{3Ca}\partial_{xxxx} \right] \tilde{h}. \tag{89}$$

So, similarly to what has been done in section 3.3, the dispersion relation becomes

$$\forall k \in \mathbb{N}, \quad \lambda_k = -2ik + k^2 \left(\frac{8}{15}(Re - Re_0) - \frac{\alpha}{3} - \frac{k^2}{3Ca} \right). \tag{90}$$

We can see in figure 15 a plot of the effect of the proportional control on the λ_k for the air jet and liquid blowing and suction controls.

To stabilize the system in the linear approximation for any type of perturbations, we want

$$\forall k \in \mathbb{N}^*, \mathfrak{R}(\lambda_k) < 0,$$

which is equivalent (except for $k = 0$) to take
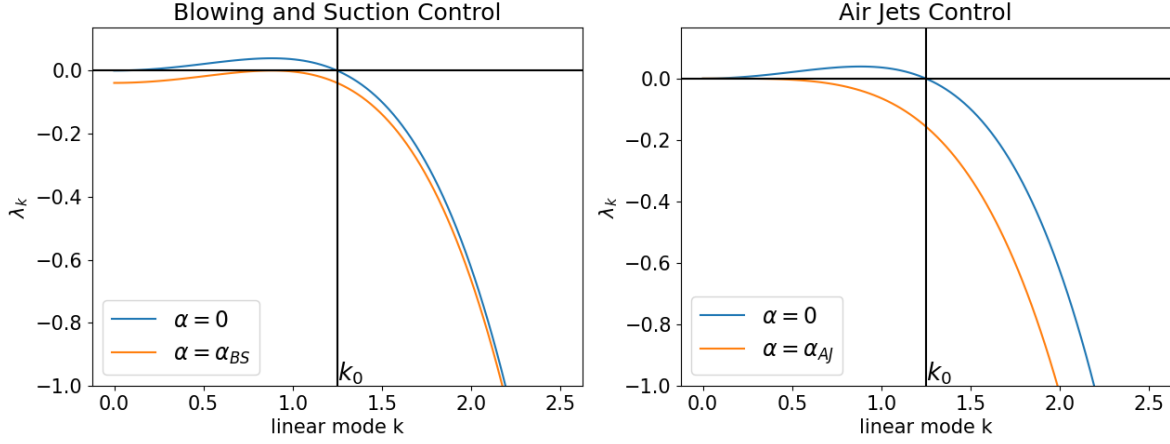
$$\boxed{\alpha > \alpha_{AJ} := \frac{24}{15}(Re - Re_0).} \tag{91}$$

42

Figure 15: Plots of $\mathfrak{R}(\lambda(k))$ with $\alpha = 0$ and $\alpha = \alpha_{AJ}$ in the left plot, and $\alpha = 0$ and $\alpha = \alpha_{BS}$ in the right plot. Without the control, there exist exponential growing mode for $k \leq k_0$ with k_0 defined in (47). When the theoretical proportional control is applied, we can see that while the curve is just shifted down along the y-axis in the blowing and suction case, its curvature is changed in the air jet case. That was expected as the α coefficient appears as a second order term (i.e in k^2) so it has an influence on the second derivative of $\mathfrak{R}(\lambda(k))$, hence on its curvature.

In comparison, the coefficient α for liquid blowing and suction in paper [16] was

$$\alpha_{BS} := \frac{16Ca(Re - Re_0)^2}{75}. \tag{92}$$

We see that α_{AJ} do not depend on the capillary number and depends linearly on $(Re - Re_0)$, while α_{BS} depends linearly on Ca and quadratically on $(Re - Re_0)$. Physically speaking, is it surprising that the Capillary number appears in the blowing and suction mechanism but not in the air jets one as the air jet interact directly with the liquid surface. Mathematically speaking, we remark that any proportional control which only affects the second derivative will not depend on Ca [7]. Let us now evaluate these coefficient with the value that we used with the numerical scheme verification (58). We have

$$\alpha_{AJ} = \frac{24}{15}(5 - 0.72) = 6.9, \quad \alpha_{BS} = \frac{16 \times 1.10^{-3}}{75}(5 - 0.72)^2 = 0.0039. \tag{93}$$

We notice that $\alpha_{AJ} \gg \alpha_{BS}$ because of the Capillary number Ca which is very small. Hence, theoretically, the blowing and suction method seems to be less expensive than the air jet one. Nevertheless, as said in section 1, it is more difficult to set up in real life

---

[7]Only a control on the even derivative will have an effect in the amplitude in this linear theory, whereas the control on the odd derivative could act on the speed of the wave (the imaginary part of λ_k). Maybe that a control on the 4th derivative could be better than the air jet or blowing and suction one.

systems as on would need to drill holes in the plane. In the blowing and suction case, the coefficient α_{AJ} is the maximal coefficient where there exists a mode k such that $\Re(\lambda(k)) \geq 0$. For an α above that threshold, all the modes are exponentially decreasing and the solution flattens towards the Nusselt solution. It is not the case of the air jet actuation method where we will always have $\lambda_0 = 0$. Indeed, a non zero order 0 mode would imply having a different mass as the one of the Nusselt solution as we add something whose average is different than zero. Therefore, it was expected that $\lambda_0 = 0$ because the air jet actuation conserves the mass of the liquid so its mean height will not change. We can see in (15) that the control changes the curve of the dispersion relation but not its value on $k = 0$.

Discrete system. In both air jet and blowing/suction cases, the coefficient α is not enough to stabilize the real discrete system. Indeed, this coefficient was built with the assumption that we have actuators on all the points of the continuous domain (called "distributed control" in [16]). However, a continuous actuation is not possible (at least to the author's knowledge) and we want to have few actuators (around 5) so that it can be convenient for industrial purposes.

Therefore, we go back to the discrete system (75) that we set in the previous section . The idea of proportional control is that all actuators have the same proportional answer α to the height. Therefore, the gain matrix is here

$$K = \alpha I_{k,N_x} \in \mathcal{M}_{k,N_x}. \tag{94}$$

Hence, the poll placement problem (70) becomes:

$$\boxed{\text{Find } \alpha_{AJ}^{num} \in \mathbb{R}_+, \quad \forall v \in Sp(A + \alpha_{AJ}^{num}BI_{k,N_x}), \Re(v) < 0,} \tag{95}$$

with α_{AJ}^{num} the solution of (95).

5.3.2 Numerical simulations for normal and positive part proportional control

We carry out simulations for the proportional control, then, we only keep the positive part of it, and compare the result to the those of the LQR control. We take

$$\boxed{N_x = 512, k = 5} \tag{96}$$

for all the simulations.

For the normal proportional control, we tested $\alpha = \alpha_{AJ} = 6.8$ from the linear theory, and $\alpha_{AJ}^{num} = 14.92$, computed by solving (95) with the `scipy.optimize` function. We found that $\alpha = \alpha_{AJ}$ wasn't sufficient to stabilize the system, in contrary to α_{AJ}^{num}, yet with a weak dampening rate (around 1.7).

For the normal proportional control, we found that we can reach the same dampening rate d_r as the LQR control strategy with about the same costs κ_u (quantities in

red in the table 4). We tested higher values of α and saw that we can reach very high dampening rates. For example for $\alpha = 100$, $d_r \approx 30$ with $\kappa_u \approx 6$.

Then, we carried out simulations by only taking the positive part of the proportional control, the obtained result being presented in the table 5. We found again that we reach the same dampening rate than the one obtained with LQR control method ($d_r \approx 12$). We write in red in table 5 where we reach these dampening rates. The positive proportional control is more expensive than the positive LQR control, with κ_u around

$$\frac{6 - 4.5}{4} = 37.5\%.$$

Moreover, for the same dampening rate (e.g $\alpha = 100$ in table 5 and $\beta = 0,95$ in 3), with see that the maximum blowing amplitude as far more intense in the proportional case than the LQR one, by

$$\frac{30 - 17}{17} \approx 76\%.$$

Table 4: Proportional control: array of the cost κ_u and the dampening rate d_r with different α

α	$\alpha_{AJ} = 6.8^8$	9	11	13	$\alpha^{num}_{AJ} = 14.92$	17	19	21
κ_u	X	4.3888	4.4924	4.1929	3.7112	3.3083	3.0667	2.9399
d_r	-2.6	-0.8	-0.3	0.9	1.7	2.6	3.6	4.6
$\max_{\substack{1 \leq i \leq N_t \\ 1 \leq j \leq k}} |u^i_j|$	3.5306	3.1347	3.6007	4.2053	4.7741	5.3686	5.9275	6.4711
α	23	25	27	29	31	33	35	37
κ_u	2.8883	2.8838	2.9094	2.9546	3.0132	3.0813	3.1563	3.2365
d_r	5.7	6.7	7.8	8.8	9.9	10.9	12	13
$\max_{\substack{1 \leq i \leq N_t \\ 1 \leq j \leq k}} |u^i_j|$	6.9996	7.5627	8.1678	8.7728	9.3778	9.9828	10.5878	11.1929
α	39	41	43	45	47	49	51	53
κ_u	3.3207	3.4081	3.4979	3.5898	3.6833	3.7783	3.8745	3.9718
d_r	14.1	15.1	16.1	17.1	18.1	19.1	20.1	21
$\max_{\substack{1 \leq i \leq N_t \\ 1 \leq j \leq k}} |u^i_j|$	11.7979	12.4029	13.0079	13.6130	14.2180	14.8230	15.4280	16.0330

All in all, we carried out numerical simulations to test proportional control actuation on the Benney system. For the normal proportional control, we found that we could reach the same dampening rate than LQR control. The strategy using the positive part of the proportional feedback control seemed to be more expensive than the strategy using the positive part of LQR control. Hence, as we are interested in blowing only air jets control, proportional control seems to be less effective than LQR control. Moreover, the LQR methodology could be enhanced by finding a better ζ_+ as $\zeta_+ = 2$ isn't necessary the best value to stabilize the Benney system.

Table 5: Positive part of proportional control: Array of the cost κ_u and the dampening rate d_r with different α

α	$\alpha_{AJ} = 6.8$ [9]	9	11	13	$\alpha_{AJ}^{num} = 14.92$	17	25
κ_u	2.3581	4.8036	4.9509	5.4336	5.8049	6.0576	5.8105
d_r	-2.6	-0.8	-0.3	-0.1	0.026	0.2	1.1
$\max_{\substack{1 \leq i \leq N_t \\ 1 \leq j \leq k}} \lvert u_j^i \rvert$	9.6991	5.3815	4.6559	4.6774	4.7634	5.3583	7.5627
α	33	40	50	70	80	90	100
κ_u	5.0504	4.7140	4.6527	5.0808	5.3877	5.7204	6.0724
d_r	2.3	3.6	5.4	9.0	10.7	12.2	13.7
$\max_{\substack{1 \leq i \leq N_t \\ 1 \leq j \leq k}} \lvert u_j^i \rvert$	9.9828	12.1004	15.1255	21.1757	24.2008	27.2260	30.2511

Finally, let us note that these results probably highly rely on the initial condition (58) that we took. Ideally, it would have been better to carry out these tests on different configurations of Re and Ca, and also different initial conditions (e.g travelling waves or non sinusoïdal steady states).

5.4   Positive control system

We saw that we could stabilize the system with blowing-only air jets. We constructed the proportional and LQR control from the linear theory with a space and time continuum (i.e no discretization) so these methods are backed with analytical results. However, we do not have any theoretical backup for the positive controls that we built by taking the positive part of the proportional and LQR controls. In this section, we try to find a gain matrix that would keep the control positive and make the Benney system asymptotically stable. We find a system of linear inequalities that would give the wanted solution. We try to solve it numerically by reformulating it as a classic QP (Quadratic Programming) optimization problem.

5.4.1   Positive control system

We want to build a control in a way that we can prove analytically that the height will stay positive and the control too. First, we reformulate the linear control system (75) using the initial height $h = 1 + \delta \tilde{h}$:

$$\frac{dh}{dt} = \delta \frac{d\tilde{h}}{dt} = \delta \left[A\tilde{h} + Bu \right] \tag{97}$$

$$\overset{(\tilde{h} = \frac{h-1}{\delta})}{=} Ah + \delta Bu - A \begin{pmatrix} 1 \\ \vdots \\ 1 \end{pmatrix}. \tag{98}$$

As A is a derivation matrix, its evaluation is null on constants with respect to space so $A \begin{pmatrix} 1 \\ \vdots \\ 1 \end{pmatrix} = 0$. Consequently, so we have the new control system

$$
\begin{cases}
\dfrac{dh}{dt} = Ah + Bu = (A + BK)h \\
h(t = 0) = h_0
\end{cases}
\tag{99}
$$

It gives again an exponential system with matrix A+KB. The difference with problem (69) is that we have here a sign constraint on h and u since they have to stay positive, so just having A+KB being a Hurwitz matrix is not sufficient. Let us then define the notion of positive system.

<u>Definition and theorem:</u> Positive system and Metzler matrix
Let $A \in \mathcal{M}_n$. The exponential system

$$
\begin{cases}
\dfrac{dh}{dt} = Ah \\
h(0) = h_0
\end{cases}
\tag{100}
$$

is said to be <u>positive</u> according to [14], if

$$
h_0 \in \mathbb{R}_+ \implies \forall t \geq 0, h(t) \geq 0.
\tag{101}
$$

Furthermore, the system is asymptotically stable if and only if

$$
\forall (i,j) \in [|1,n|]^2, i \neq j \implies A_{i,j} \geq 0.
$$

This type of matrix are called <u>Metzler matrix</u>

Therefore, to have a positive and asymptotically stable system, we would need that A+KB is a Hurwitz and Metzler matrix.

To ensure that the control is also positive, [14] gives a way to build the gain matrix K by solving this system of linear inequalities:

$$
\text{Find } d \in \mathbb{R}^n, (z_j)_{1 \leq j \leq n} \in (\mathbb{R}^k)^n,
\begin{cases}
Ad + \delta B \displaystyle\sum_{i=1}^{n} z_i < 0 \\
d > 0 \\
z_i \geq 0 \quad \forall i \in [|1,n|] \\
a_{ij} d_j + \delta b_j^T z_j \geq 0 \quad \forall i \neq j
\end{cases}
.
\tag{102}
$$

The gain matrix is finally given by

$$
\boxed{K = (d_1^{-1} z_1 | \dots | d_n^{-1} z_n).}
\tag{103}
$$

47

Here, according to the same paper, the first and inequalities ensure that $A+\delta BK$ is Hurwitz, the last that it is Metzler, and the third one that the control will be positive as the gain matrix will have non negative coefficient. Indeed, if $A + \delta BK$ is Metzler and Hurwitz, the system (99) is positive and asymptotically stable. Therefore, as the state of the system is non negative, the feedback control will also be non negative.

5.4.2 Reformulation into a QP optimization problem

As we did not find any solver for linear inequalities system, we reformulate (102) as a constrained Quadratic Programming Optimization problem.

First, we construct the matrices $H \in \mathcal{M}_{n,n+nk}$ and $M \in \mathcal{M}_{n^2,n+nk}$ which will translate the first (one of the two conditions for matrix to be Hurwitz) and last lines (the only condition for the matrix to be Metzler) of the system.

Let us set

$$v = \begin{pmatrix} d \\ z_1 \\ \vdots \\ z_n \end{pmatrix}.$$

Then,

$$Ad + \delta B \sum_{i=1}^{n} z_i < 0 \Leftrightarrow Hv < 0, \quad \text{with} \quad H = (A, \delta B, -, \delta B) \in \mathcal{M}_{n,n+nk}.$$

As of M, we take $s = (i-1)n + j \in [|1, n^2|]$ so that we characterise the couple $(i,j) \in [|1,n|]^2$ only with s by

$$i_s = 1 + \lfloor \frac{s-1}{n} \rfloor, \quad j_s = (s-1)\%n + 1.$$

Next,

$$(a_{ij}d_j + \delta b_i z_j > 0 \quad \forall i \neq j) \Leftrightarrow Mv > 0$$

with

$$M_{sr} = \begin{cases} 0 \text{ if } i_s = j_s \\ a_{i_s j_s} \text{ if } r = j_s \\ \delta b_{i_s, r-(n+(j_s-1)k)} \text{ if } r \in [|n + (j_s-1)k+1, n+j_s k|] \end{cases}.$$

Then, let

$$v_{tot} = \begin{pmatrix} v \\ v \end{pmatrix}.$$

The Metzler and Hurwitz conditions are then :

$$Gv_{tot} < 0, \quad \text{with } G = \begin{pmatrix} -M & 0 \\ 0 & H \end{pmatrix}.$$

48

Then, we enforce that $v_{tot,c} = v_{tot,c+n+nk}$ (i.e that $v_{tot} = \begin{pmatrix} v \\ v \end{pmatrix}$) with:

$$A_{QP}v_{tot} = 0_{n+nk}, \quad \text{with } A_{QP} = (Id_{n+nk}, -Id_{n+nk}).$$

Finally we have this Optimization problem:

$$\begin{aligned} \min_{v_{tot} \in \mathbb{R}^{2(n+nk)}} \quad & v_{tot}^T S v_{tot} \\ s.t \quad & Gv_{tot} < h := 0 \in \mathbb{R}^{n^2+n} \\ & A_{QP}v_{tot} = b := 0 \in \mathbb{R}^{n+nk} \\ & v_{tot} > lb := 0 \in \mathbb{R}^{2(n+nk)} \end{aligned} \tag{104}$$

with S such that we minimize the $(z_i)_{i \in [|1,N_x|]}$ to have a small cost for the control as the gain matrix would have small component.

Numerical Solving. To solve (104), We use the python package `qpsolvers` that can be found in this Github repository.

We did not manage to find a solution which was Hurwitz and Metzler in the same time, even for small values of N_x. Concretely, the first part of the vector v_{tot} outputted by the solver would encode a Hurwitz Matrix, while the second part would encode a Metzler matrix, but never both of the properties. Moreover, the solver would output very small values (around 10^{-14}) with d being significantly smaller than the $(z_i)_{i \in [|1,N_x|]}$, so the control would be too large and make the numerical scheme bug. This problem of small values could be maybe be solved by taking another objective function, like

$$(v_{tot} - 1)^T S(v_{tot} - 1)$$

with $S = I_d$ for example.

6 Conclusion

In this report we studied the stabilization of a falling liquid film with blowing only air jets and found controls that could stabilize the Benney equation, a reduced-order model of the Navier-Stokes system.

In part 2, we studied numerically the KS equation with different values of the instability parameter $\nu = (2\pi/L)^2$ and tried to interpretate the observed behaviour by analysing the Fourier modes of the unkown u. We saw that the numerical solution had a rich behaviour, from stabilizing towards a non-steady state to turning into a travelling wave. Then, in section 3, we derived the Benney equation (41). More precisely, we used the thin film approximation and made an hypothesis on the scale of the Reynolds number Re, the Capillary number Ca, but also on the normal and tangential stress induced by the air jets N_s and T_s, where T_s was neglected. Then, in section 4, we introduced a numerical scheme to solve numerically the Benney equations. We carried out

several tests to fix the parameter of the simulation namely the order of the Backward Differentiation Formula scheme N_{BDF} and the number of space steps N_x (the number of time steps N_t being deduced from N_x by (51)). We tested the convergence of two spatial methods, the finite difference and spectral method, and then compared them to see if they where giving the same results which was indeed the case. Finally, in section 5, we built two blowing only air jet strategies that stabilize successfully the Benney system. The first strategy was to compute the LQR (Linear Quadratic Regulator) control for the Benney system and take its postive part multiplied by some scalar ζ_+. The second was to carry out a proportional control and take its positive part too. We found out that proportional control seems to be more costly than LQR control for the same dampening rate in the context of blowing-only actuation, especially when it comes to the maximum of the control amplitudes. However, if we do not take the positive part, the proportional control seems to be as efficient as the LQR control for some values of the proportional control coefficient α. We also tried another control method by changing our system into a positive control system which are system with a positive state at all time t. We found from [14] a system of linear inequalities that we changed into a QP (Quadratic Programming) optimization problem to solve it. However, we didn't manage to find a solution numerically with the solver.

A The code

A.1 Scheme for the KS equation

We study the truncated system. In the code, we update the cosinus and sinus part separately. Here, for convenience, we just detail the part for the cosinus update but the non linearities depends also on the sinus part.

As the scheme needs the values of the Fourier modes for the first p time steps, we compute them with a classic implicit Euler scheme on the linearity, and explicit on the non-linearity. This starting scheme is exactly the scheme we use for $p_{BDF} = 1$.

We make and abuse of notation by calling the discrete operators only for the cosinus parts of the fourier transform A and B. We also denote p instead of p_{BDF} as the formulas are a bit heavy.

Therefore:

$$AU^{n,M} = ((\lambda_j + \frac{1}{\nu})u_j^c(ndt)))_{1 \leq j \leq M}, \quad B(U^{n,M}) = ((\frac{1}{\nu}u_j^c(ndt) + F_j^{d,c}))_{1 \leq j \leq M}.$$

We denote $u^{c,n} = (u_j^c(ndt))_{j \in [|1,d|]}$ We call $\Lambda := Diag(\lambda_1, \ldots, \lambda_d)$ the diagonal matrix with λ_j, so

$$A = \Lambda + \frac{1}{\nu}I_d.$$

From the numerical scheme, we get that

$$(\alpha_p I_d + dtA)U^{n+p,M} = ((\alpha_p + \frac{dt}{\nu})I_d + dt\Lambda)U^{n+p,M}$$

$$= -\sum_{i=0}^{p-1} \alpha_i U^{n+i,M} + dt \sum_{i=0}^{p-1} \gamma_i B(U^{n+i,M}).$$

So, only for the cosinus part:

$$((\alpha_p + \frac{dt}{\nu})I_d + dt\Lambda)u^{c,n+p} = -\sum_{i=0}^{p-1} \alpha_i u^{c,n+i} + dt \sum_{i=0}^{p-1} \gamma_i(\frac{1}{\nu}u^{c,n+i} + F^{c,n+i,M})$$

i.e

$$u^{c,n+p} = ((\alpha_p + \frac{dt}{\nu})I_d + dt\Lambda)^{-1}(-\sum_{i=0}^{p-1} \alpha_i u^{c,n+i} + dt \sum_{i=0}^{p-1} \gamma_i(\frac{1}{\nu}u^{c,n+i} + F^{c,n+i,M})) \in \mathbb{R}^d.$$

Finally, we "vectorize" the expression above. We introduce some matrices $\mathcal{U}^{d,c}$ and $\mathcal{F}^{d,c}$. Their row are for each time steps and their columns for each Fourier modes. We denote the extracted vector from $\mathcal{F}^{d,c}$ coordinate i to j included $\mathcal{F}_{i,j}^{d,c}$.

$$H^{c,n+p} = ((\alpha_p + \frac{dt}{\nu})I_d + dt\Lambda)^{-1}(-\underline{\alpha}_{p-1}^T . \mathcal{U}_{n,n+p-1}^{c,M} + dt\underline{\gamma}_{p-1}^T . (\frac{1}{\nu}\mathcal{U}_{n,n+(p-1)}^{c,M} + \mathcal{F}_{n,n+(p-1)}^{c,M})) \in \mathbb{R}^M.$$

with

$$\mathcal{U}_{n,n+(p-1)}^{c,M}, \mathcal{F}_{n,n+(p-1)}^{c,M} \in \mathcal{M}_{p-1,M}, \quad \underline{\alpha}_{p-1} = (\alpha_0, ..., \alpha_{p-1})$$

and

$$\underline{\gamma}_{p-1} = (\gamma_0, ..., \gamma_{p-1}).$$

Which gives finally the expression of u^s at the new time step:

$$u^{c,n+p} = Diag((\frac{1}{\alpha_p + \frac{dt}{\nu} + dt\lambda_j})_{j \in [|1,M|]})((\frac{dt}{\nu}\underline{\gamma}_{p-1}^T - \underline{\alpha}_{p-1}^T).\mathcal{U}_{n,n+p-1}^{c,M} + dt\underline{\gamma}_{p-1}^T . \mathcal{F}_{n,n+(p-1)}^{c,M}) \in \mathbb{R}^M.$$

(105)

Likewise (just changing the non-linearities),

$$u^{s,n+p} = Diag((\frac{1}{\alpha_p + \frac{dt}{\nu} + dt\lambda_j})_{j \in [|1,M|]})((\frac{dt}{\nu}\underline{\gamma}_{p-1}^T - \underline{\alpha}_{p-1}^T).\mathcal{U}_{n,n+p-1}^{s,M} + dt\underline{\gamma}_{p-1}^T . \mathcal{F}_{n,n+(p-1)}^{s,M}) \in \mathbb{R}^M.$$

(106)

The 0th Fourier mode is taken null. Therefore, we have all the Fourier modes at time (n+p)dt.

B The governing equations

The undimensionnalised Navier Stokes equation (26) are the Navier Stokes equation in the non-Newtonian and incompressible case.

B.1 KBC and mass conservation

The Kinematic Boundary Condition (KBC) is

$$\frac{Df}{Dt} = \left[\frac{\partial}{\partial t} + (\underline{u}.\underline{\nabla})\right] f = 0 \text{ with } f(x,y,z) = z - h(x,y,t).$$

So it gives

$$h_{,t} = w - uh_{,x} - vh_{,y}.$$

We denote $I_x(h(x,y,t),x,t) := q_x(x,y,t) = \int_0^{h(x,y,t)} u(x,y,z,t)dz$. Likewise, $I_y(h(x,y,t),x,t) := q_y(x,y,t) = \int_0^{h(x,y,t)} v(x,y,z,t)dz$.

So, as u(z=0) = v(z=0) = 0 (no slip),

$$
\begin{cases}
q_{x,x} = h_{,x}\partial_1 I_x + 1 \times \partial_2 Ix + 0 = h_{,x}[u(x,y,h,t) - 0] + \displaystyle\int_0^h u_{,x}(x,u,z,t)dz \\[4mm]
q_{y,y} = h_{,y}\partial_1 I_y + 1 \times \partial_2 Iy + 0 = h_{,y}[v(x,y,h,t) - 0] + \displaystyle\int_0^h v_{,y}(x,u,z,t)dz
\end{cases}.
$$

So

$$
\underline{\nabla}.\underline{q} = h_{,x}u + h_{,y}v + \int_0^h (u_{,x} + v_{,y})dz. \tag{107}
$$

Finally (KBC + Incompressibility), $\underline{\nabla}.\underline{q} = w - h_{,t} - \int_0^h w_{,z}dz = w - h_{,t} - (w(x,y,h,t) - 0)$

so

$$
\boxed{h_{,t} + \underline{\nabla}.\underline{q} = 0.} \tag{108}
$$

B.2 Dynamic boundary conditions

Let us prove the Dynamic Boundary Conditions (28) the 3D case and then return to the 2D one:

According to Kaliadasis book [9]:

$$
(\underline{\underline{\sigma_l}} - \underline{\underline{\sigma_g}}).\underline{n} = \gamma\kappa\underline{n} \tag{109}
$$

with $\kappa = \underline{\nabla}.\underline{n}$ and $\underline{n} = \frac{1}{\sqrt{1+h_{,x}^2+h_{,y}^2}}(-h_{,x}, -h_{,y}, 1)$ the normal vector pointing towards gas from the liquid which is the convention we're using in this document. Let's be careful about that convention and some potential sign errors as some papers take the other direction (i.e gas $\to$ liquid) n.

Hence, with the notation we have introduced in the paper,

$$
\underline{\underline{\sigma_l}}.\underline{n} + \underline{s_g} = \gamma\kappa\underline{n}.
$$

We define

$$
N_s = \underline{s_g}.\underline{n}, \quad T_{si} = \underline{s_g}.\underline{t_i}, i \in \{x,y\},
$$

with

$$
\underline{t_x} = \frac{1}{\sqrt{1+h_{,x}^2}}(1,0,h_{,x}), \quad \underline{t_y} = \frac{1}{\sqrt{1+h_{,y}^2}}(0,1,h_{,y}).
$$

The family $(\underline{n}, \underline{t_x}, \underline{t_y})$ is normalized, orthogonal and direct.

(109).$\underline{n}$ at $y = h$ gives:

53

$$\gamma\kappa|\underline{n}|^2 = \underline{n}.\underline{\underline{\sigma}}_l.\underline{n} + \underline{n}.\underline{s}_g$$

$$= \underline{n}.\left(-p_l\underline{\underline{I}} + \mu_l(\underline{\underline{\nabla}}^T u_l + \underline{\underline{\nabla}} u_l)\right).\underline{n} + N_s$$

$$= \frac{1}{1 + h_{,x}^2 + h_{,y}^2}(-h_{,x}, -h_{,y}, 1)\left(-p_l\underline{\underline{I}} + \mu_l(\underline{\underline{\nabla}}^T u_l + \underline{\underline{\nabla}} u_l)\right)(-h_{,x}, -h_{,y}, 1)^T + N_s,$$

with $(u_l = u_g := u$ at $y = h)$

$$-p_l\underline{\underline{I}} + \mu_l(\underline{\underline{\nabla}}^T u_l + \underline{\underline{\nabla}} u_l) = -p_l\underline{\underline{I}} + \mu_l \begin{pmatrix} 2u_{,x} & u_{,y} + v_{,x} & u_{,z} + w_{,x} \\ \cdot & 2v_{,y} & v_{,z} + w_{,y} \\ \cdot & \cdot & w_{,z} \end{pmatrix}.$$

And, according to Kalliadasis' book [9]:

$$\gamma\kappa|\underline{n}|^2 = \gamma\kappa = \frac{\gamma}{(1 + h_{,y}^2 + h_{,x}^2)^{3/2}}\left[h_{,yy}(1 + h_{,x}^2) + h_{,xx}(1 + h_{,y}^2) - 2h_{,y}h_{,x}h_{,yx}\right].$$

Hence (after non dimensionalisation...)

$$\frac{\mu_l U_l}{h_l}\left[-p_l + \frac{2}{1 + h_{,x}^2 + h_{,y}^2}[\ldots] + N_s\right] = \frac{\gamma}{h_l}\frac{1}{(1 + h_{,y}^2 + h_{,x}^2)^{3/2}}[\ldots]$$

which gives finally, in 3D:

$$-p_l + \frac{2}{1 + h_{,x}^2 + h_{,y}^2}\left[h_{,x}^2 u_x + h_{,y}^2 + h_{,y}^2 v_y + w_{,z} + h_{,x}h_{,y}(v_{,x} + u_{,y})\right.$$

$$\left. - h_{,x}(w_{,x} + u_{,z}) - h_{,y}(w_{,y} + v_{,z})\right] + N_s \tag{110}$$

$$= \frac{1}{Ca}\frac{1}{(1 + h_{,y}^2 + h_{,x}^2)^{3/2}}\left[h_{,yy}(1 + h_{,x}^2) + h_{,xx}(1 + h_{,y}^2) - 2h_{,x}h_{,y}h_{,yx}\right].$$

In 2D $(x \leftrightarrow x, y \leftrightarrow z$, and y ignored), we retrieve the normal part of (37) i.e:

$$\boxed{-p_l + \frac{2}{1 + h_{,x}^2}(u_{,x}h_{,x}^2 - h_{,x}(u_{,y} + v_{,x}) + v_{,y}) = \frac{1}{Ca}\frac{h_{,xx}}{(1 + h_{,x}^2)^{3/2}} - N_s.}$$

<u>Tangential Case.</u> (109).$\underline{t}_x$ gives:

$$\underline{t}_x.(\underline{\underline{\sigma}}_l + \underline{s}_g).\underline{n} = \underline{t}_x.\underline{\underline{\sigma}}_l.\underline{n} + T_{sx} = \gamma\kappa\underline{t}_x.\underline{n} = 0 \quad \text{(orthogonal)}$$

$$\frac{1}{\sqrt{1 + h_{,x}^2 + h_{,y}^2}\sqrt{1 + h_{,x}^2}}(1, 0, h_{,x})\left[-p_l\underline{\underline{I}} + \mu_l(\underline{\underline{\nabla}}^T u_l + \underline{\underline{\nabla}} u_l)\right](-h_{,x}, -h_{,y}, 1)^T + T_{sx} = 0$$

So (undimensionalisation & computation..)

$$\frac{1}{\sqrt{1+h_{,x}^2+h_{,y}^2}\sqrt{1+h_{,x}^2}}\Big[2h_{,x}(w_{,z}-u_{,x})-h_{,y}(u_{,y}+v_{,x})$$
$$+ (1-h_{,x}^2)(u_{,z}+w_{,x})-h_{,x}h_{,y}(v_{,z}+w_{,y})\Big] = -T_{sx}.$$

Hence, in 2D, we retrieve the tangential part of (37) i.e:

$$\boxed{\frac{(v_{,x}+u_{,y})(1-h_{,x}{}^2)+2h_{,x}(v_{,y}-u_{,x})}{1+h_{,x}^2} = -T_s.}$$

It's the same for $-T_{sy}$ with some indices swapping. Let us note that the choice of the direction of $\underline{n}$ can change the sign $\pm$ before the T_{sx} if we do not always take an direct orthonormal triplet (N_s, T_{sx}, T_{sy}). Therefore, it is important to pay attention to the physical meaning of these quantities.

C Derivation of the reduced-order models

C.1 Benney equation

The Benney equation is derived from the non-dimensional Navier-Stokes equation by making a change of variable and performing order-1 asymptotics in ϵ on it. A more detailed the computations in the blowing and suction of liquid case can be found in the appendix of[15]. The only difference is that the the control (denoted "f" in the cited paper) is taken null here and N_s (denoted "p_a" in the cited paper) is not a constant.

The chosen change of variable is

$$X = \epsilon x, \quad T = \epsilon t, \quad v = \epsilon w, \quad Ca = \epsilon^2 \tilde{Ca}.$$

The approximated quantities are then:

$$\begin{aligned} u &= u_0 + \epsilon u_1 + O(\epsilon^2), \quad v = v_0 + \epsilon v_1 + O(\epsilon^2) \\ p &= p_0 + \epsilon p_1 + O(\epsilon^2), \quad q = q_0 + \epsilon q_1 + O(\epsilon^2) \end{aligned} \tag{111}$$

The Navier-Stokes equations (26) become

$$\begin{cases} \epsilon Re(u_{,T} + u u_{,X} + w u_{,y}) = -\epsilon p_{l,x} + 2 + \epsilon^2 u_{,XX} + u_{,YY} \\ \epsilon^2 Re(w_{,T} + u w_{,X} + w w_{,y}) = -\epsilon p_{l,y} + 2\cot(\theta) + \epsilon^3 w_{,XX} + \epsilon w_{,YY} \\ \qquad\qquad u_{,X} + w_{,y} = 0 \end{cases} \tag{112}$$

The Kinematic boundary condition becomes

$$\begin{cases} p_l - \dfrac{2}{1+\epsilon^2 h_{,X}^2}\Big(\epsilon w_{,y} + \epsilon^3 u_{,x} h_{,x}^2 - \epsilon h_{,x}(\epsilon^2 w_{,x} + u_{,y})\Big) = -\dfrac{h_{,XX}}{\tilde{C}a(1+\epsilon^2 h_{,X}^2)^{3/2}} + N_s \\ (\epsilon w_{,X} + u_{,y})(1 - \epsilon^2 h_{,X}{}^2) + 2\epsilon^2 h_{,X}(w_{,y} - u_{,X}) = 0 \end{cases}.$$

(113)

The mass conservation is

$$h_{,T} + q_{,X} = 0$$

and the boundary conditions are

$$u = 0, v = 0, \quad \text{at y=0}.$$

The order 0 for the pressure is given by the y-axis projection of the NS equation and the tangential KBC. We take $Ca = O(\epsilon^2)$ and N_s of the same order as the liquid pressure p_l so that surface and external pressure effects appears in the order 0 pressure of the liquid.

With first order computations using the equations above, we have that

$$u_0 = y(2h - y), \quad p_{l,0} = N_s + 2(h-y)cot(\theta) - \frac{h_{,XX}}{\tilde{C}a}, \quad w = -y^2 h_{,X}. \quad (114)$$

The 0-order flux is then

$$q_0(x,t) = \int_0^h u_0(x,y,t)dy = \frac{2h^3}{3}$$

Then, we find $u_{1,yy}$ with the Navier-Stokes equation. We integrate using the boundary condition and tangential part of the KBC, and we find

$$u_1 = \frac{yp_{l0,X}}{2}(y - 2h) + Re\Big[h_{,T}(\frac{y^3}{3} - yh^2) + \frac{2hh_{,X}}{3}(\frac{y^4}{4} - h^3 y)\Big].$$

The first order flux is then

$$q_1 = \int_0^h u_1 dy = -\frac{h^3 p_{l0,X}}{3} + \epsilon Re\frac{8h_{,X}h^6}{15} + O(\epsilon). \quad (115)$$

Finally, the total flux at order 1 is

$$q = q_0 + \epsilon q_1 + O(\epsilon^2) = \frac{2h^3}{3} - \frac{\epsilon h^3 p_{l0,X}}{3} + \epsilon Re\frac{8h^6 h_{,X}}{15},$$

When rescaled we have:

$$\boxed{q(x,t) = \frac{2h^3}{3} - \frac{h^3 p_{l0,x}}{3} + Re\frac{8h^6}{15},} \quad (116)$$

which is equation (39) that we use in the report.

C.2 The KS equation

We present briefly the derivation of the KS equation that we take from the section 1.2 of the thesis of Dr. Susana Gomes [5]. We did not carry out the computations again this time as it is just to have an idea of what the variable u in (4) is constructed.

From the uncontrolled Benney equation (33), we take $h(x,t) = 1 + \epsilon u(\xi, t)$ where we made a change of variable to place ourselves in a moving reference frame of unitary speed, with $\xi = x - t, \tau = \epsilon t$. It gives

$$U_{,\tau} + 4UU_{,\xi} + \left(\frac{8Re}{15} - \frac{2}{3}cot(\theta)\right)U_{,\xi\xi} + \frac{1}{3\tilde{C}a}U_{,\xi\xi\xi\xi} = 0.$$

Let us consider this new change of variable

$$U = \frac{1}{60}\sqrt{\frac{3\tilde{C}a8^3(Re - Re_0)^3}{15}}u, \quad \xi = \sqrt{\frac{5}{8\tilde{C}a(Re - Re_0)}}X, \qquad (117)$$

$$\tau = \frac{75}{8^2\tilde{C}a(Re - \frac{Re_0}{5}))^2}T, \qquad (118)$$

with $Re_0 = \frac{5cot(\theta)}{4}$, the unstable Reynolds number defined in (45). It gives

$$\boxed{u_{,T} + u_{,XXXX} + u_{,XX} + uu_{,X} = 0, \quad u(x + L) = u(x)},$$

i.e the KS-equation (1) that we considered in section 2. Let us note that this last change of variable does not work for $Re \leq Re_0$.

References

[1] Georgios Akrivis and Michel Crouzeix. "Linearly implicit methods for nonlinear parabolic equations". In: *Mathematics of Computation* 73 (Jan. 2004), pp. 613–635.

[2] Georgios Akrivis and Demetrios Papageorgiou. "Linearly implicit methods for a semilinear parabolic system arising in two-phase flows". In: *IMA Journal of Numerical Analysis 299−321 [Received on January* 31 (Jan. 2011). DOI: 10.1093/imanum/drp034.

[3] Fabian Denner et al. "Solitary waves on falling liquid films in the inertia-dominated regime". In: *Journal of Fluid Mechanics* 837 (2018), pp. 491–519. DOI: 10.1017/jfm.2017.867.

[4] Fabian Denner et al. "Solitary waves on falling liquid films in the inertia-dominated regime". In: *Journal of Fluid Mechanics* 837 (2018), pp. 491–519. DOI: 10.1017/jfm.2017.867.

[5]   Susana Gomes. "Control theory for infinite dimensional dynamical systems and applications to falling liquid film flows". PhD thesis. Imperial College London, 2016.

[6]   Susana N. Gomes, Demetrios T. Papageorgiou, and Grigorios A. Pavliotis. *Stabilising nontrivial solutions of the generalised Kuramoto-Sivashinsky equation using feedback and optimal control*. 2015. arXiv: 1505.06086 [math.OC]. URL: https://arxiv.org/abs/1505.06086.

[7]   Oscar A. Holroyd, Radu Cimpeanu, and Susana N. Gomes. *Linear quadratic regulation control for falling liquid films*. 2023. arXiv: 2301.11379 [math.OC]. URL: https://arxiv.org/abs/2301.11379.

[8]   Oscar A. Holroyd, Radu Cimpeanu, and Susana N. Gomes. *Stabilisation of falling liquid films with restricted observations*. 2024. arXiv: 2407.06906 [math.OC]. URL: https://arxiv.org/abs/2407.06906.

[9]   Serafim Kalliadasis et al. "Falling Liquid Films". In: 2011. URL: https://api.semanticscholar.org/CorpusID:117042076.

[10]   Yoshiki Kuramoto. "Diffusion-Induced Chaos in Reaction Systems". In: *Progress of Theoretical Physics Supplement* 64 (Feb. 1978), pp. 346–367. ISSN: 0375-9687. DOI: 10.1143/PTPS.64.346. eprint: https://academic.oup.com/ptps/article-pdf/doi/10.1143/PTPS.64.346/5293041/64-346.pdf. URL: https://doi.org/10.1143/PTPS.64.346.

[11]   D. Lunz and P. D. Howell. "Dynamics of a thin film driven by a moving pressure source". In: *Phys. Rev. Fluids* 3 (11 Nov. 2018), p. 114801. DOI: 10.1103/PhysRevFluids.3.114801. URL: https://link.aps.org/doi/10.1103/PhysRevFluids.3.114801.

[12]   D.M. Michelson and G.I. Sivashinsky. "Nonlinear analysis of hydrodynamic instability in laminar flames—II. Numerical experiments". In: *Acta Astronautica* 4.11 (1977), pp. 1207–1221. ISSN: 0094-5765. DOI: https://doi.org/10.1016/0094-5765(77)90097-2. URL: https://www.sciencedirect.com/science/article/pii/0094576577900972.

[13]   Chinasa Juliet Ojiako et al. "Deformation and dewetting of liquid films under gas jets". In: *Journal of Fluid Mechanics* 905 (2019). URL: https://api.semanticscholar.org/CorpusID:210839383.

[14]   M. Ait Rami and F. Tadeo. "Controller Synthesis for Positive Linear Systems With Bounded Controls". In: *IEEE Transactions on Circuits and Systems II: Express Briefs* 54.2 (2007), pp. 151–155. DOI: 10.1109/TCSII.2006.886888.

[15]   Alice B. Thompson, Dmitri Tseluiko, and Demetrios T. Papageorgiou. "Falling liquid films with blowing and suction". In: *Journal of Fluid Mechanics* 787 (2016), pp. 292–330. DOI: 10.1017/jfm.2015.683.

[16]   Alice B. Thompson et al. "Stabilising falling liquid film flows using feedback control". In: *Physics of Fluids* 28.1 (Jan. 2016). ISSN: 1089-7666. DOI: 10.1063/1.4938761. URL: http://dx.doi.org/10.1063/1.4938761.